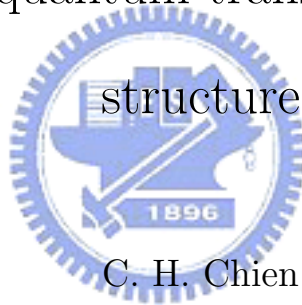


Effects of decoherence and Rashba-type spin-orbit
interaction on quantum transport in mesoscopic



C. H. Chien

October 12, 2005

Contents

1	introduction	1
1.1	Motivations	1
1.2	A guiding tour to this thesis	2
1.3	Derivation for the Landauer-Buttiker Formalism	3
2	Decoherence effect in a serial quantum point contact structure	6
2.1	Experimental result of quantum point contact in serial	6
2.2	Formulation of quantum point contact in serial and theory of decoherence	8
2.3	Numerical results and discussion	17
3	Quantum transport through a Rashba-type spin-orbit open quantum dot: in the absence of subband mixing	23
3.1	Solving the eigen state in channel with Dresselhaus and Rashba spin-orbit interaction in the absence of subband mixing	23
3.2	Matching boundary condition and scattering method	26
3.3	Numerical result and discussion	33
4	Quantum transport through a Rashba-type spin-orbit open quantum dot: including subband mixing	37
4.1	Solving the eigen state in channel with Dresselhaus and Rashba spin-orbit interaction including subband mixing	37
4.2	Matching boundary condition and scattering method	45

CONTENTS

5	Spin-dependent current and numerical result	55
6	Conclusion and Future work	63



List of Figures

2.1	Destruction of coherence in double quantum point contacts (QPCs) in series.	7
2.2	Experimental results of double quantum point contacts (QPCs) in series. $G^* = \frac{1}{(R_{12}-R_2)}$. R_{12} is total resistance. L is the distance from QPC1 to QPC2.	8
2.3	Our model of quantum point contact in serial	9
2.4	wave function representation in one quantum point contact	10
2.5	Model of the inelastic coupler	12
2.6	Phase randomizing scatter between two QPC, outgoing amplitudes are related to the incoming amplitudes through S-matrix, while amplitudes to the left of the inelastic scatter are related to the amplitudes at the right side through the transfer matrix.	16
2.7	Conductance is plotted against the width of QPC	18
2.8	Total Conductance of two QPCs in series plotted against the width of QPC2. The width of QPC1 is fixed. L_q the length of QPC is $1 \times \frac{1}{k_f}=9.2$ nm and they are separated with $L = 3 \times \frac{1}{k_f}=27.6$ nm. ε is decoherence strength. Energy of incident electron is 1.5 with unit $E^* = \frac{\hbar^2 \pi^2 k_F^2}{2m^*}$ eV. Number of subband is 40 in our approximation.	19
2.9	Conductance of QPC2 plotted against the width of QPC2.	20
2.10	Total conductance plotted against incident energy under $w_2 = 2$.	21
2.11	Total conductance plotted against incident energy under $w_2 = 4$.	22

LIST OF FIGURES

3.1	The model of Rashba-type spin-orbit open quantum dot	27
3.2	Open quantum dot in the absence of spin-orbit interaction	33
3.3	Open quantum dot with spin-orbit interaction in absence of subband mixing	34
3.4	Open quantum dot with spin-orbit interaction in absence of subband mixing and asymmetric structure.	35
3.5	the ratio of flipping spin plotted against the rashba coupling in the open quantum dot.	36
4.1	Assume a plain wave propagating in angle of θ	38
4.2	Assume one incident wave has one reflected wave	39
4.3	Add another reflected wave to fit boundary condition	40
4.4	Dispersion relation	44
4.5	The model of open quantum dot.	46
5.1	Open quantum dot with spin-orbit interaction in the absence of subband mixing under asymmetric structure	55
5.2	Open quantum dot including spin-orbit interaction and subband mixing under asymmetric structure	56
5.3	Spin precession distribution and the number of density in the open quantum dot	57
5.4	Open quantum dot including spin-orbit interaction with $\alpha_D=0.05$ which is stronger than Fig. 5.2	58
5.5	Spin precession distribution and the number of density in the open quantum dot with $\alpha_D=0.05$	59
5.6	Open quantum dot with spin-orbit interaction in the absence of subband mixing under symmetric structure	60
5.7	Open quantum dot including spin-orbit interaction and subband mixing under asymmetric structure	61

LIST OF FIGURES

5.8 Spin precession distribution and the number of density in the open quantum
dot with $\alpha_D=0.05$ under symmetric structure 62



Chapter 1

introduction

1.1 Motivations

In the recent years research in semiconductor physics has been focused on the emerging field of spintronics. Among the most prominent devices proposals is the spin-field-effect transistor (FET) due to Datta and Das [1]. This proposal uses the Rashba spin-orbit (s.o) coupling to perform controlled rotations of spins of electrons passing through an FET-type device. This particular spin-orbit interaction is due to inversion-symmetry of the confining potential and is of the form [2]

$$\mathcal{H}_R = \frac{\alpha}{\hbar} (p_x \sigma_y - p_y \sigma_x)$$

where \vec{p} is the momentum of the electron confined in a two-dimensional geometry, and $\vec{\sigma}$ the vector of Pauli matrices. The coefficient α is tunable in strength by the external gate of the FET. Not only one subject to spin-orbit interaction of the Rashba but also of Dresselhaus type [3] we will apply. The latter is present in semiconductors lacking bulk inversion symmetry. When restricted to a two dimensional semiconductor nanostructure with appropriate growth geometry, this is coupling of the form [4, 5]

$$\mathcal{H}_D = \frac{\beta}{\hbar} (p_x \sigma_x - p_y \sigma_y)$$

where the coefficient β is determined by the semiconductor material and the geometry of the sample. Tune the Rashba (via proper gating) and the Dresselhaus terms so that they have equal strength $\alpha = \beta$. In this case, we quite generally below that the electron spinor is k independent in two dimensions.

Then we have an idea. Special case is $|\alpha| = |\beta|$, which leads to the cancellation of the k dependence the eigenstates, exhibits universal direction ($\pm\pi/4$ for $\alpha = \mp\beta$). And In the absence of the Dresselhaus term, spin direction is perpendicular to k direction. If we propose have a device with spin k -independent lead and k -dependent dot, shall we have spin-dependent current?

In our research, we met D.r hsu's group and discuss the problem of double quantum point contacts (QPCs) in series. We find out we can support them some brief theoretical results via applying our experience in solving open quantum dot. So, why not just do it?



1.2 A guiding tour to this thesis

In next section of this chapter, we introduce the Lansauer-Buttiker formula and a long controversy on it. This is the fundamental theory about next thesis. Extend these concepts to more complicated geometrical structures in which phase coherence is preserved and the description in terms of quantum flux is important. Such systems include quantum point contacts as well as more complicated quantum waveguide structure in 2 and 3 dimensions. To generalize our formalism for treating current flow through such systems, we go back to an early formalism, which has now become standard in the parlance of nanostructure transport.

In chapter2, the experimental status in the realization of the destruction of coherence in double quantum point contacts in series is reviewed. This experimental result is proposed by K. M. Liu , W. R. Chen, Y. M. Lin , and S. Y. Hsu Low Temperature Laboratory, Department of Electrophysics, National Chiao Tung University. Then We propose a theoretical physical model to simulate their device and extend the model of inelastic

scatter with complete randomization in 1 dimension to 2 dimensions.

The numerical results, discussion, and theoretical calculation of the Rashba spin-orbit effect on the transport characteristics in a open quantum dot via lead has both Dresselhaus and Rashba spin-orbit interaction are shown in in chapter 3 and 4. In chapter 3, we neglect the subband-mixing in open quantum dot to get analytic form. In chapter 4, we include subband-mixing in our calculation and get numerical form.

1.3 Derivation for the Landauer-Buttiker Formalism

We adapt the Landauer-Buttiker approach to calculate the conductance across the source and drain.

In 1957, Landauer [6] proposed the novel point of view that transport should be viewed as a consequence of incident flux. Later in 1970 [7], he further proposed that the conductance of a one-dimensional conductor sandwiched between two phase-randomizing reservoirs is given by

$$G = \frac{2e^2}{h} \frac{T}{R}$$

where T and R are the transmission and reflection coefficients of the conductor treated as a single complex scattering center, and only one spin direction is included.

The formula was rediscovered in 1980 by Anderson et al [8] by employing it in a rigorous formulation of the scaling theory of localization. Since then Landauer formula caught the attention of wider community [9]. Nevertheless, another version of conductance $G = \frac{2e^2}{h} T$ was obtained by Economou and Soukoulis later in 1981 [10]. The answer was that they pertain to different physical quantities [11]

This started a long controversy on "which of the Landauer formula is correct?"

For the original Landauer formula, $G = \frac{I}{\mu_A - \mu_B} T$, where μ_A and μ_B are the chemical potentials on the L.H.S. and R.H.S. of the barrier. However, the conductance formula by Economou et. al. is $G_c = \frac{I}{\mu_1 - \mu_2} T$. Here, G_c is the conductance measured between the

two outside reservoirs. The ambiguity of the two Landauer formulas was clarified by Imry in 1986.

Apart from the controversy which is confusing before mid-80s, Landauer formula faced another practical difficulties as it is restricted in single channel one-dimensional case only.

However, the Multichannel Landauer formula were proposed by Buttiker on 1985 [12] and later in 1986 [13], he predicted a symmetry property in a four-probe experiment under a magnetic flux and was successfully observed by Benoit et.al. [14] Since the confirmation of the formula, it has been a concrete foundation for quantum transport theory. In short, Landauer's great insight that conduction in solids can be thought as a scattering problem, and Buttiker brilliant extension of the multichannel formula has become the key understanding of quantum transport in mesoscopic system. Hence, It is also now well known as Landauer-Buttiker formula.

Next, we try to derive the multichannel Landauer-Buttiker Formula starting from single channel case. Full reference is available on the original paper of M. Buttiker et. al. [12]

Assume that there are two reservoir of electrochemical potential μ_1 and μ_2 respectively and the two end of 1D channel; and, there is a barrier in between the reservoirs.

If we add a small bias at the two reservoir, then the difference of electrochemical potential between the reservoir will be $\mu_1 - \mu_2 = \Delta\mu$. And, the transmission probability of an electron from reservoir 1 to reservoir 2 can be calculated by Quantum Mechanics as T . As both side of electrons from reservoir 1 to 2 or reservoir 2 to 1 cancel out each other, only those transmitted electrons in between $\Delta\mu$ contribute to the current density J from reservoir 1 to 2. In 1D, $J = I$.

Therefore the current, I can be written as:

$$I = -2e \frac{dn}{dE} (\mu_1 - \mu_2) T \frac{\hbar k_F}{m}$$

Note that $\frac{dn}{dE} (\mu_1 - \mu_2)$ is the number of states per unit length that are injected from

reservoir 1; the velocity is equal to $\frac{\hbar k_F}{m}$; and, the number 2 refers to spin factor. Besides, density of state per unit length in 1D is

$$\frac{dn}{dE} = \frac{dk}{2\pi/L} \frac{1}{(\hbar^2 k_F)/m} = \frac{m}{\hbar^2 k_F} \frac{1}{2\pi}$$

Therefore, $I = -\frac{2e}{h} (\mu_1 - \mu_2) T$. Moreover, the definition of conductance, $G = \frac{I}{V}$, and $\mu_1 - \mu_2$ is given by the voltage across V , so that $\mu_1 - \mu_2 = -eV$. As a result, we have

$$G = \frac{I}{V} = \frac{-2e/h (eV) T}{V} = \frac{2e^2}{h} T$$

For the $N \times N$ multichannel system, we have the incident channel as n , the transmission probability to m as T_{nm} , and the reflection probability to m as R_{nm} . Therefore, the total transmission probability, T_n from the n th channel is $\sum_{m=1}^N T_{nm}$; and the total current, I_{tot} would be $\sum_n^N I_n$.

$$I_n = -\frac{2e}{h} (\mu_1 - \mu_2) \sum_{m=1}^N T_{nm}$$

and,

$$I_{tot} = -\frac{2e}{h} (\mu_1 - \mu_2) \sum_n^N \sum_{m=1}^N T_{nm}$$

Subsequently, the conductance for $N \times N$ multichannel system would be:

$$G = \frac{2e^2}{h} \sum_n^N \sum_{m=1}^N T_{nm}$$

Chapter 2

Decoherence effect in a serial quantum point contact structure

2.1 Experimental result of quantum point contact in serial



Here we report some experimental result of destruction of coherence in double quantum point contacts (QPCs) in series. We want to propose an theoretical model to simulate the experimental result by K. M. Liu , W. R. Chen, Y. M. Lin , and S. Y. Hsu Low Temperature Laboratory, Department of Electrophysics, National Chiao Tung University. The device as shown in Fig. 2.1 The main workhorse in regards to experimental measurements is the split-gate structure fabricated on a high-mobility electron gas structure. For zero gate bias, the 2DEG exists essentially everywhere in the space between the two Ohmic contacts. With a negative bias applied to the two Schottky contact gates, the 2DEG is depleted underneath as well as laterally from geometric edge of the gates. In the narrow region between the two split-gates, a 1DEG is formed. The density of the 1DEG decrease as the gate bias is made more negative until it eventually disappears between the split gates. The length of the 1DEG is defined by the width of the gate contacts and the shape of depletion regions around the contacts. Such split-gate structure are often referred to

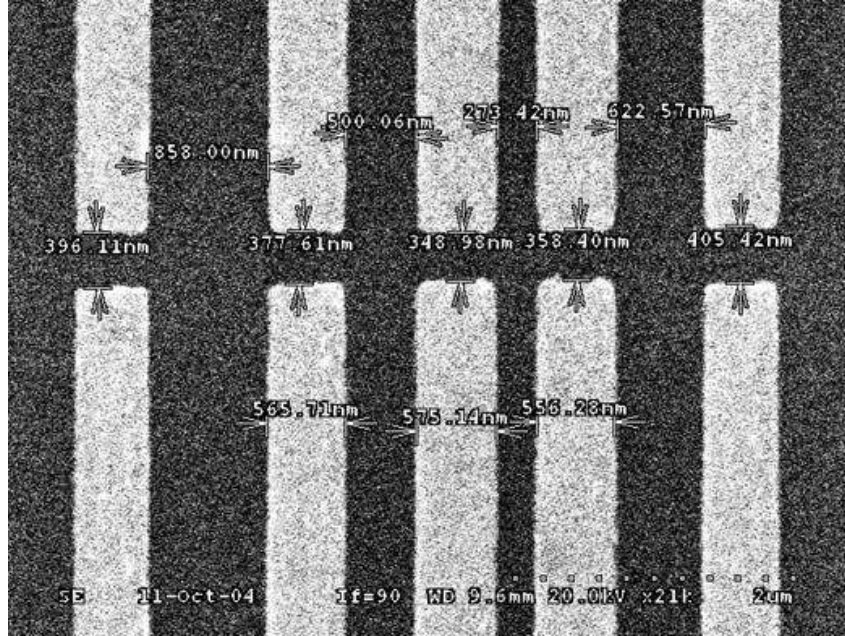


Figure 2.1: Destruction of coherence in double quantum point contacts (QPCs) in series.

quantum point contacts.

In our device, several pairs of split gate are fabricated. Via choosing different pair of split gate, we can observe the distance of double QPCs how to influence the total conductance by choosing which pair of split gate.

GaAs/AlGaAs 0.3K	
carrier density n_s	$1.88 \times 10^{11} \text{cm}^{-2}$
mobility μ	$0.8 \times 10^6 \text{cm}^2/\text{Vs}$
Fermi wavelength λ_f	57.8 nm
mean free path l_e	$5.9 \mu\text{m}$

QPCs is formed by applying negative bias on the split metal gates that are fabricated the top of $GaAs - Al_xGa_{1-x}As$ hetrostrucure. This table shows the parameter of $GaAs - Al_xGa_{1-x}As$ we use.

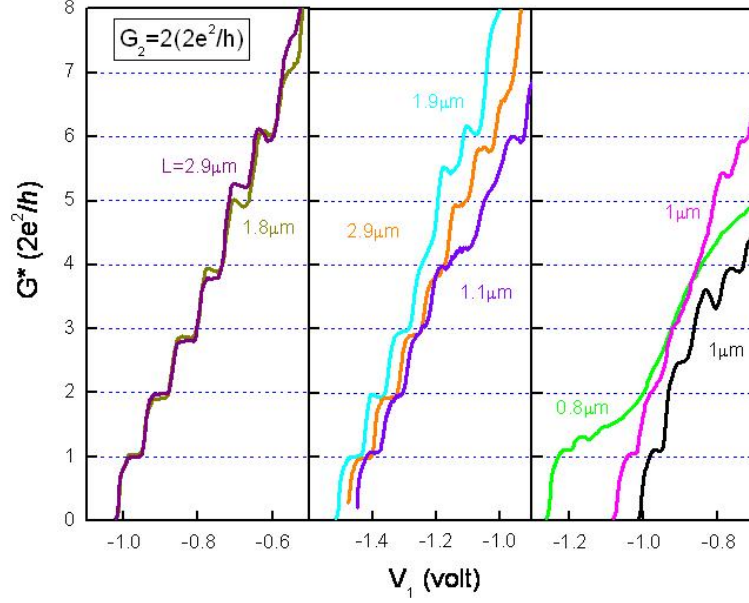


Figure 2.2: Experimental results of double quantum point contacts (QPCs) in series. $G^* = \frac{1}{(R_{12}-R_2)} \cdot R_{12}$ is total resistance. L is the distance from QPC1 to QPC2.

Fig. 2.2 is G^* plotted against the negative voltage on split gate 1. Choose the voltage on the other split gate satisfy its conductance is $G_2 = 2$ with unit $\frac{2e^2}{h}$. In this figure, G^* behaves as quantized conductance when L approaches to mean free path $l_e = 5.9\mu m$. So we want to propose a theoretical model to simulate the decoherence strength between double QPCs in series.

2.2 Formulation of quantum point contact in serial and theory of decoherence

We consider uniform constriction to simulate the QPC structure. our dimensionless hamiltonian can be written as: $H = -\frac{\hbar^2}{2m} \left(\frac{\partial^2}{\partial x^2} + \frac{\partial^2}{\partial y^2} \right) + V_c(x, y)$

We can separate our problem into two parts-QPC1 and QPC2. Then, we will connect the scattering matrix by an inelastic scattering matrix. Through match boundary condition, we can get the relationship of transmission and reflection coefficients of QPC1 and

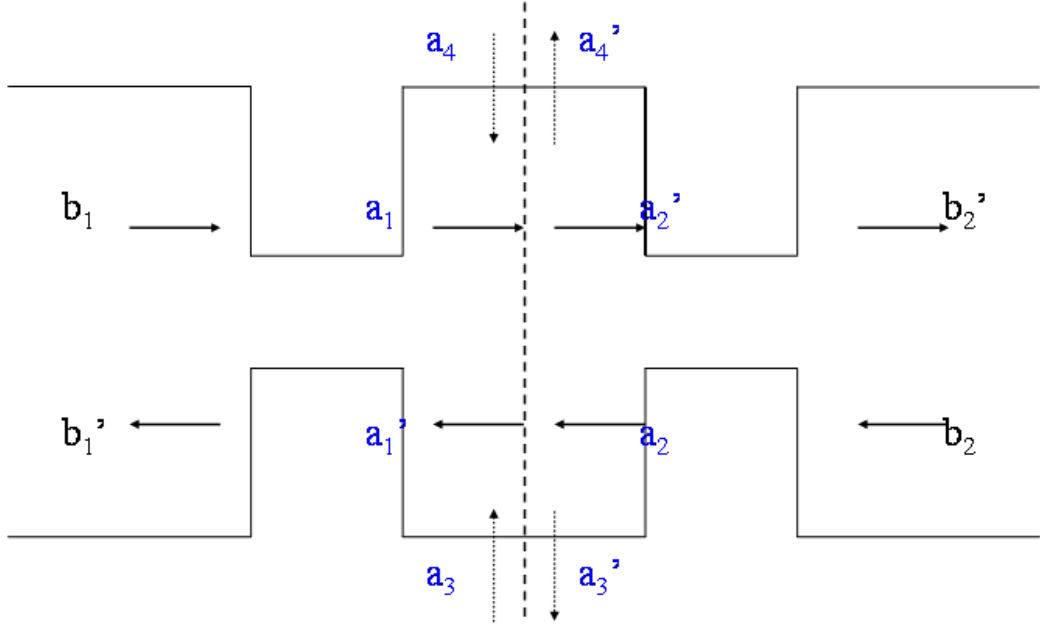


Figure 2.3: Our model of quantum point contact in serial

get the scattering matrix of QPC1.

$$M \cdot \begin{bmatrix} r_n \\ t_n \\ A_n \\ B_n \end{bmatrix} = \begin{bmatrix} V_1 \\ V_2 \\ V_3 \\ V_4 \end{bmatrix} \quad M = \begin{bmatrix} M_{11} & M_{12} & M_{13} & M_{14} \\ M_{21} & M_{22} & M_{23} & M_{24} \\ M_{31} & M_{32} & M_{33} & M_{34} \\ M_{41} & M_{42} & M_{43} & M_{44} \end{bmatrix} \quad (2.1)$$

To construct scattering matrix, we need a complete basis to expand the wave function. In hard wall confinement, we choose Eq. (2.2) and Eq. (2.3) to be our basis as usual.

$$\phi_n(y) = \sqrt{\frac{2}{w_r}} \cdot \sin\left(\frac{n\pi y}{w_r}\right) \quad (2.2)$$

$$\tilde{\phi}_n(y) = \sqrt{\frac{2}{w_3}} \cdot \sin\left(\frac{n\pi y}{w_3}\right) \quad (2.3)$$

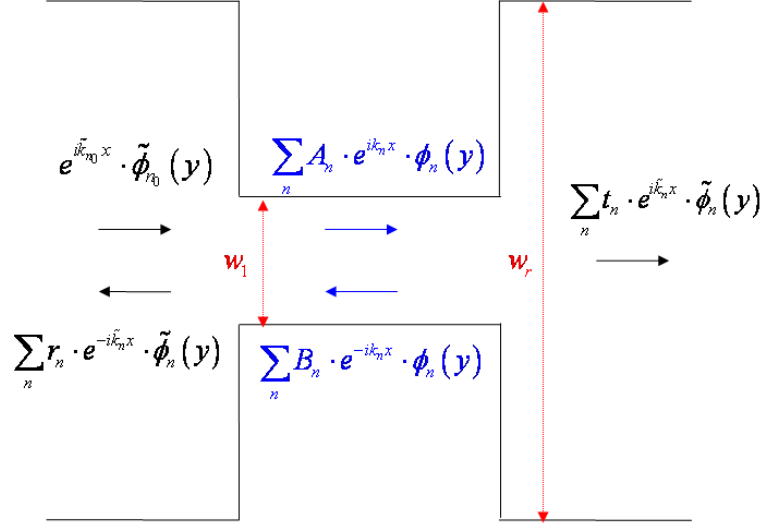


Figure 2.4: wave function representation in one quantum point contact

For an electron incident from subband $n = n_0$, the scattering wave function would be of the form.

$$\psi_1(x, y) = e^{i\tilde{k}_{n_0}x} \cdot \tilde{\phi}_{n_0}(y) + \sum_n r_n \cdot e^{-i\tilde{k}_n x} \cdot \tilde{\phi}_n(y) \quad (2.4)$$

$$\psi_2(x, y) = \sum_n [A_n \cdot e^{ik_n x} + B_n \cdot e^{-ik_n x}] \cdot \phi_n(y) \quad (2.5)$$

$$\psi_3(x, y) = \sum_n t_n \cdot e^{ik_n x} \cdot \phi_n(y) \quad (2.6)$$

where n is the subband index, ϵ is energy, and $\tilde{k}_n = \sqrt{\epsilon - \frac{n^2}{w_r}}$. The energy unit is taken to be $E^* = \frac{\hbar^2 \pi^2 k_F^2}{2m^*}$, and length unit is $a^* = \frac{1}{k_F}$.

Match wave function continuous at $x = L_1$ and $x = L_2$:

$$\begin{aligned} & \tilde{\phi}_{n_0}(y) \cdot e^{i\tilde{k}_{n_0}L_1} + \sum_n r_n \cdot \tilde{\phi}_n(y) \cdot e^{-i\tilde{k}_n L_1} \\ &= \sum_n [A_n \cdot e^{ik_n L_1} + B_n \cdot e^{-ik_n L_1}] \cdot \phi_n(y) \end{aligned} \quad (2.7)$$

$$\begin{aligned} & \sum_n [A_n \cdot e^{ik_n L_2} + B_n \cdot e^{-ik_n L_2}] \cdot \phi_n(y) \\ &= \sum_n t_n \cdot \delta_{n',n} \cdot e^{i\tilde{k}_n L_2} \cdot \tilde{\phi}_n(y) \end{aligned} \quad (2.8)$$

Match slope of wave function continuous at $x = L_1$ and $x = L_2$:

$$\begin{aligned} & \tilde{k}_{n_0} \cdot \tilde{\phi}_n(y) \cdot e^{i\tilde{k}_{n_0}L_1} + \sum_n r_n \cdot (-\tilde{k}_n) \cdot \tilde{\phi}_n(y) \cdot e^{-i\tilde{k}_nL_1} \\ = & \sum_n [A_n \cdot e^{ik_nL_1} - B_n e^{-ik_nL_1}] \cdot k_n \cdot \phi_n(y) \end{aligned} \quad (2.9)$$

$$\begin{aligned} & \sum_n [A \cdot e_n^{ik_nL_2} - B_n \cdot e^{-ik_nL_2}] \cdot k_n \cdot \phi_n(y) \\ = & \sum_n t_n \cdot \delta_{n',n} \cdot \tilde{k}_n \cdot e^{i\tilde{k}_nL_2} \cdot \tilde{\phi}_n(y) \end{aligned} \quad (2.10)$$

Multiplying Eq. (2.7) and Eq. (2.8) by $\int_d^{d+w_1} \phi_{n'}(y) dy$, we have:

$$\begin{aligned} & \delta_{n',n_0} \cdot e^{i\tilde{k}_{n_0}L_1} + \sum_n r_n \cdot \delta_{n',n} \cdot e^{-i\tilde{k}_nL_1} \\ = & \sum_n [A_n \cdot e^{ik_nL_1} + B_n \cdot e^{-ik_nL_1}] \cdot \int_d^{d+w_1} \tilde{\phi}_{n'}(y) \cdot \phi_n(y) dy \end{aligned} \quad (2.11)$$

$$\begin{aligned} & \sum_n [A_n \cdot e^{ik_nL_2} + B_n \cdot e^{-ik_nL_2}] \cdot \int_d^{d+w_2} \tilde{\phi}_{n'}(y) \cdot \phi_n(y) dy \\ = & \sum_n t_n \cdot \delta_{n',n} \cdot e^{i\tilde{k}_nL_2} \end{aligned} \quad (2.12)$$

Multiplying Eq. (2.9) and Eq. (2.10) by $\int_d^{d+w_1} \phi_{n'}(y) dy$, we have:

$$\begin{aligned} & \tilde{k}_{n_0} \cdot e^{i\tilde{k}_{n_0}L_1} \cdot \int_d^{d+w_1} \phi_{n'}(y) \cdot \tilde{\phi}_{n_0}(y) dy \\ + & \sum_n r_n \cdot (-\tilde{k}_n) \cdot e^{-i\tilde{k}_nL_1} \cdot \int_d^{d+w_1} \phi_{n'}(y) \cdot \tilde{\phi}_n(y) dy \\ = & \sum_n [A_n \cdot e^{ik_nL_1} - B_n e^{-ik_nL_1}] \cdot k_n \cdot \delta_{n',n} \end{aligned} \quad (2.13)$$

$$\begin{aligned} & \sum_n [A_n \cdot e^{ik_nL_2} - B_n \cdot e^{-ik_nL_2}] \cdot k_n \cdot \delta_{n',n} \\ = & \sum_n t_n \cdot e^{i\tilde{k}_nL_2} \cdot \tilde{k}_n \cdot \int_d^{d+w_2} \phi_{n'}(y) \cdot \tilde{\phi}_n(y) dy \end{aligned} \quad (2.14)$$

Now we can obtain the scattering matrix of QPC1 by solving Eq. (2.1) and the same

as QPC2:

$$\begin{bmatrix} a_1 \\ b'_1 \end{bmatrix} = \begin{bmatrix} S_{11} & S_{12} \\ S_{21} & S_{22} \end{bmatrix} \cdot \begin{bmatrix} b_1 \\ a'_1 \end{bmatrix} = \begin{bmatrix} T_1 & \tilde{R}_1 \\ R_1 & \tilde{T}_1 \end{bmatrix} \cdot \begin{bmatrix} b_1 \\ a'_1 \end{bmatrix} \quad (2.15)$$

$$\begin{bmatrix} b'_2 \\ a_2 \end{bmatrix} = \begin{bmatrix} S'_{11} & S'_{12} \\ S'_{21} & S'_{22} \end{bmatrix} \cdot \begin{bmatrix} a'_2 \\ b_2 \end{bmatrix} = \begin{bmatrix} T_2 & \tilde{R}_2 \\ R_2 & \tilde{T}_2 \end{bmatrix} \cdot \begin{bmatrix} a'_2 \\ b_2 \end{bmatrix} \quad (2.16)$$

In using the Landauer counting argument for defining voltage probes to introduce phase randomization, Buttiker calculated the contribution to the measured conductance due to a single-channel model of a localized inelastic scatter.

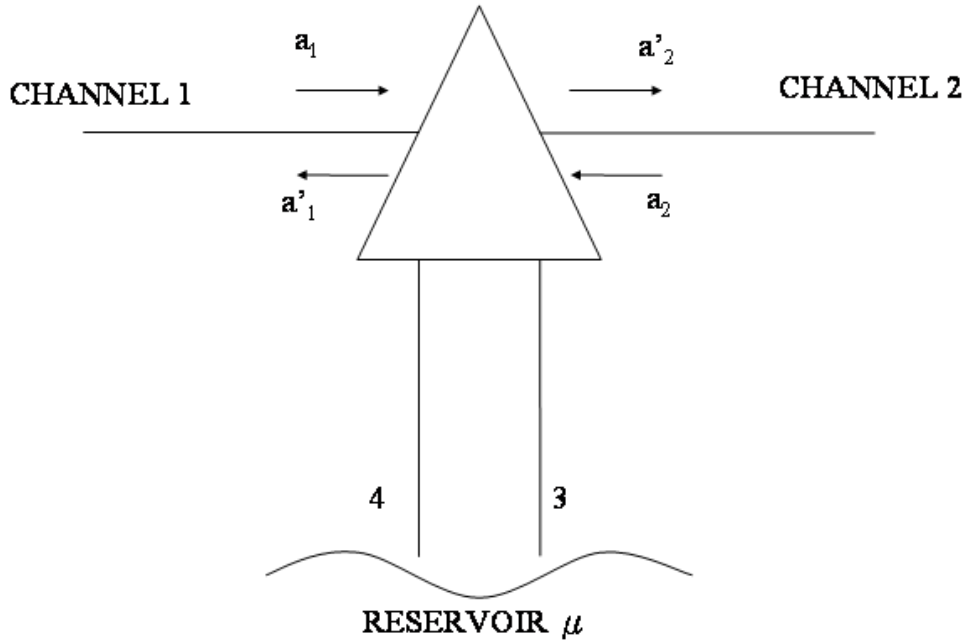


Figure 2.5: Model of the inelastic coupler

Basically an inelastic scatter at any point in a conductor is modeled by a "coupler" whose function is to connect the conductor to a thermal reservoir via a current lead with

two quantum channels, channel 3 and channel 4. Fig. 2.5. The segment of the conductor to the left of the coupler is designed as channel 1 and the segment to the right of the coupler as channel 2. Therefore in the single-channel formulation introduced by Buttiker, an inelastic scatter has four single-channel leads and is described by a unitary 4×4 S-matrix which determines the amplitudes of the outgoing waves in terms of the amplitude of the incoming waves.

A reduction of the number of distinct relevant variables for this problem can be accomplished as follows. Let S_b denote the incoherent backward scattering and S_f denote the incoherent forward scattering. For Single channel leads, these are the only scattering probabilities. Then we have,

$$S_b = T_{13} + T_{14} = |S_{13}|^2 + |S_{14}|^2 \quad (2.17)$$

$$S_f = T_{23} + T_{24} = |S_{23}|^2 + |S_{24}|^2 \quad (2.18)$$

On the other hand, the coherent process are denoted by

$$T_{c,L} = T_{21} = |S_{21}|^2, R_{c,L} = R_{11} = |S_{21}|^2, \quad (2.19)$$

$$T_{c,R} = T_{12} = |S_{12}|^2, R_{c,R} = R_{22} = |S_{22}|^2. \quad (2.20)$$

Keep current conservation and unitarity, then we have leads to relations between derived quantities as:

$$R_{c,L} + T_{c,L} + S_b = 1, \quad (2.21)$$

$$R_{c,R} + T_{c,R} + S_f = 1. \quad (2.22)$$

where $T_{c,R} = T_{c,L} = T_{21} = T_{12}$ in the absence of magnetic field.

The inelastic scatter basically randomizes the phase of the charge-carries and therefore feeds the conductor, through S_b and S_f , with incoherent carries up to energy μ , which can be determined by requiring that no net particle current flows into the reservoir. In

contrast to this zero particle flow, that inelastic scattering implies the existence of a net energy flux towards the reservoir of chemical potential μ . We have for the current in channels 3 and 4,

$$I_3 = T_{32} \cdot I(\mu_R, \mu) + T_{31} \cdot I(\mu_L, \mu) \quad (2.23)$$

$$I_4 = T_{42} \cdot I(\mu_R, \mu) + T_{41} \cdot I(\mu_L, \mu) \quad (2.24)$$

where $I(\mu_R, \beta)$ represents the saturated current values from a reservoir at chemical potential μ_β to terminal reservoir at chemical potential μ_R in the absence of any scatters.

We have for each electron spin

$$I(\mu_R, \mu) = \frac{e}{h} (\mu_R - \mu) \quad (2.25)$$

$$I(\mu_R, \mu_L) = \frac{e}{h} (\mu_R - \mu_L) \quad (2.26)$$

By requiring that $I_3 + I_4 = 0$, one readily obtains

$$\mu = \frac{\mu_R \cdot S_f + \mu_L \cdot S_b}{(S_f + S_b)} \quad (2.27)$$

Substituting the expression for μ , in terms of $(\mu_L - \mu_R)$, in the expression for $I_1 = I_2 = I$ giving by $I = T_{21} \cdot I(\mu_L - \mu_R) + S_f \cdot I(\mu - \mu_R)$, we obtain

$$G = \frac{I}{(\mu_L - \mu_R)} = T_{21} \cdot \frac{e}{h} + S_f \cdot \frac{e}{h} \frac{S_b}{(S_f + S_b)} \quad (2.28)$$

From the requirement of unitary and time-reversal symmetry in the absence of external magnetic field, we can construct the 4×4 S-matrix, which relates the scattered amplitude as functions of incident amplitudes, of an inelastic scattering process S_{in} as a symmetric

and unitary matrix

$$S_{in} = \begin{pmatrix} 0 & \sqrt{1-\varepsilon} & \sqrt{\varepsilon} & 0 \\ \sqrt{1-\varepsilon} & 0 & 0 & \sqrt{\varepsilon} \\ \sqrt{\varepsilon} & 0 & 0 & -\sqrt{1-\varepsilon} \\ 0 & \sqrt{\varepsilon} & -\sqrt{1-\varepsilon} & 0 \end{pmatrix} \quad (2.29)$$

Where ε is decoherence strength which $S_f = S_b = \varepsilon$. We can write it down as equation in series

$$\begin{cases} a'_1 = \sqrt{1-\varepsilon} \cdot a_2 + \sqrt{\varepsilon} \cdot a_3 \\ a'_2 = \sqrt{1-\varepsilon} \cdot a_1 + \sqrt{\varepsilon} \cdot a_4 \\ a'_3 = \sqrt{\varepsilon} \cdot a_1 - \sqrt{1-\varepsilon} \cdot a_4 \\ a'_4 = \sqrt{\varepsilon} \cdot a_2 + \sqrt{1-\varepsilon} \cdot a_3 \end{cases} \quad (2.30)$$

In Fig. 2.5, combining matrix equation Eq. (2.15) and Eq. (2.16), we can obtain Fig. 2.6 and Eq. (2.31)

$$\begin{bmatrix} b'_1 \\ b'_2 \\ a'_3 \\ a'_4 \end{bmatrix} = \tilde{S} \cdot \begin{bmatrix} b_1 \\ b_2 \\ a_3 \\ a_4 \end{bmatrix} \quad (2.31)$$

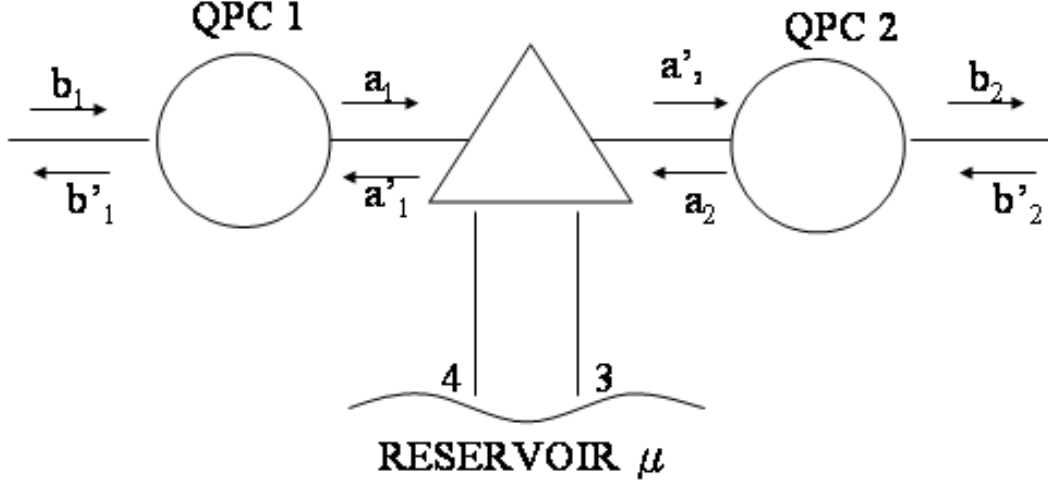


Figure 2.6: Phase randomizing scatter between two QPC, outgoing amplitudes are related to the incoming amplitudes through S-matrix, while amplitudes to the left of the inelastic scatter are related to the amplitudes at the right side through the transfer matrix.

In order to get \tilde{S} , its matrix element represents transmission rate from one channel to another channel and reflection rate. So we calculate its matrix element separately. We must notice our problem is two-dimension. So b_2 and b_1 are vectors which represent different subbands mixing. \tilde{S} is a $4n \times 4n$ unitary matrix. where n is the number of subbands we choose. Set $b_2 = a_3 = a_4 = 0$, $b_1 = \delta_{n,m}$, $b'_1 = \tilde{S}_{11}$, $b'_2 = \tilde{S}_{21}$, we obtain:

$$\left\{ \begin{array}{l} a_1 - \tilde{R}_1 \cdot \sqrt{1-\varepsilon} \cdot a_2 = T_1 \cdot \delta_{n,m} \\ \tilde{S}_{11} - \tilde{T}_1 \sqrt{1-\varepsilon} \cdot a_2 = R_1 \cdot \delta_{n,m} \\ \tilde{S}_{21} - T_2 \cdot \sqrt{1-\varepsilon} \cdot a_1 = 0 \\ -R_2 \cdot \sqrt{1-\varepsilon} \cdot a_1 + a_2 = 0 \end{array} \right. \quad (2.32)$$

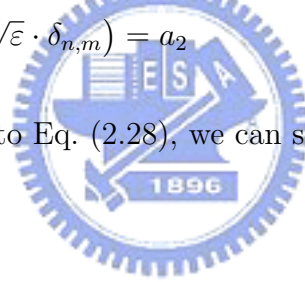
Set $b_1 = b_2 = a_4 = 0$, $a_3 = \delta_{n,m}$, $b'_1 = \tilde{S}_{13}$, $b'_2 = \tilde{S}_{23}$, we obtain:

$$\left\{ \begin{array}{l} \tilde{R}_1 \cdot (\sqrt{1-\varepsilon} \cdot a_2 + \sqrt{\varepsilon} \cdot \delta_{n,m}) = a_1 \\ \tilde{T}_1 \cdot (\sqrt{1-\varepsilon} \cdot a_2 + \sqrt{\varepsilon} \cdot \delta_{n,m}) = \tilde{S}_{13} \\ T_2 \cdot \sqrt{1-\varepsilon} \cdot a_1 = \tilde{S}_{23} \\ R_2 \cdot \sqrt{1-\varepsilon} \cdot a_1 = a_2 \end{array} \right. \quad (2.33)$$

Set $b_1 = b_2 = a_3 = 0$, $a_4 = \delta_{n,m}$, $b'_1 = \tilde{S}_{14}$, $b'_2 = \tilde{S}_{24}$, we obtain:

$$\left\{ \begin{array}{l} \tilde{R}_1 \cdot \sqrt{1-\varepsilon} \cdot a_2 = a_1 \\ \tilde{T}_1 \cdot \sqrt{1-\varepsilon} \cdot a_2 = \tilde{S}_{14} \\ T_2 \cdot (\sqrt{1-\varepsilon} \cdot a_1 + \sqrt{\varepsilon} \cdot \delta_{n,m}) = \tilde{S}_{24} \\ R_2 \cdot (\sqrt{1-\varepsilon} \cdot a_1 + \sqrt{\varepsilon} \cdot \delta_{n,m}) = a_2 \end{array} \right. \quad (2.34)$$

Put these matrix elements into Eq. (2.28), we can solve this problem to simulate experimental result.



2.3 Numerical results and discussion

In this section, we show the numerical results and discussion of two QPCs in series under decoherent effect. We take the conductance G with the unit $\frac{2e^2}{h}$. Length unit is $\frac{1}{k_f}$ nm and energy unit is $E^* = \frac{\hbar^2 \pi^2 k_F^2}{2m^*} = 0.0117$ eV. It is just as the same as previous section.

CHAPTER 2. DECOHERENCE EFFECT IN A SERIAL QUANTUM POINT CONTACT STRUCTURE

In Fig. 2.7, w_1 is the width of QPC and its length is $\text{len}(\text{QPC})$. w_r must be larger than the width of QPC to simulate width of reservoir. We choose w_r is $20 \times \frac{1}{k_f} = 194$ nm. In this figure we want to check our model can work for predict conductance of QPC. In ballistic regime, conductance of QPC is discovered a sequence of steps of the voltage of the split gate. In our model, the width of QPC is similar to the the voltage of the split gate.

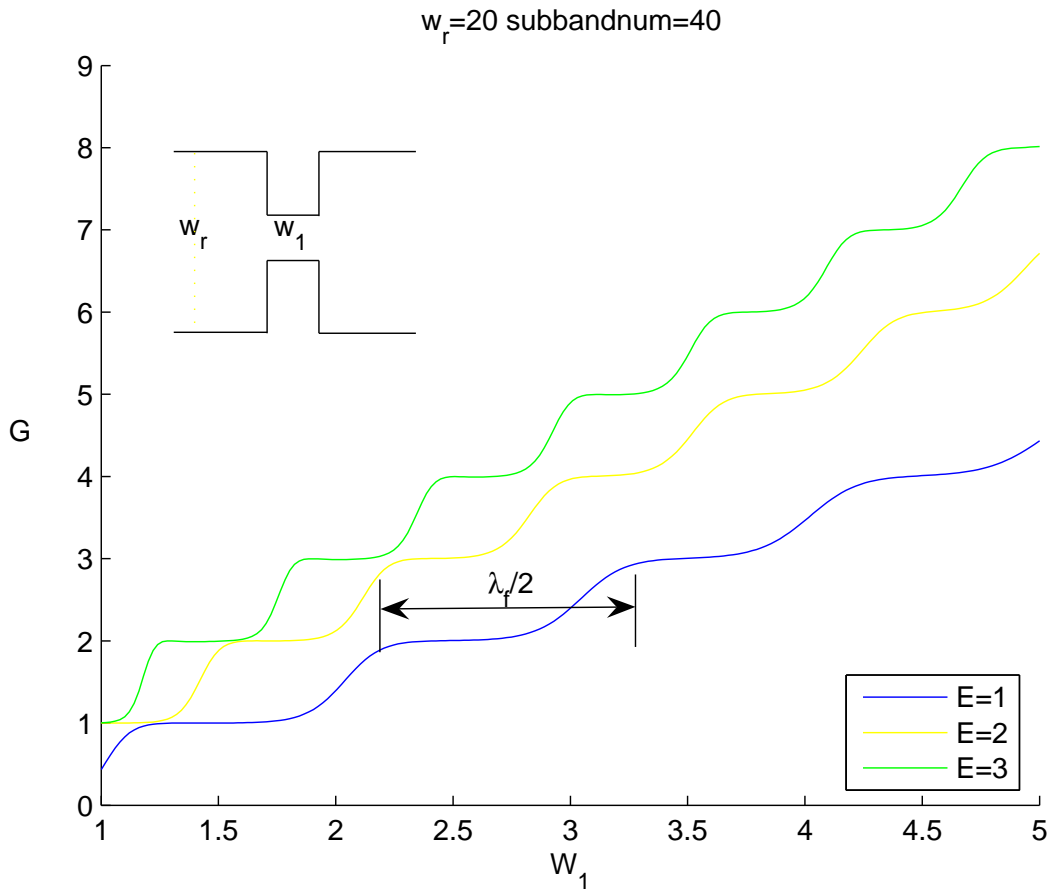


Figure 2.7: Conductance is plotted against the width of QPC

As we can see, the conductance is quantized in units of $\frac{2e^2}{h}$. The result relies on the fact of increase in number of propagating modes. The length of step is $\frac{\lambda_f}{2}$. Where λ_f is the fermi-wave length which is $\frac{2\pi}{k_f}$.

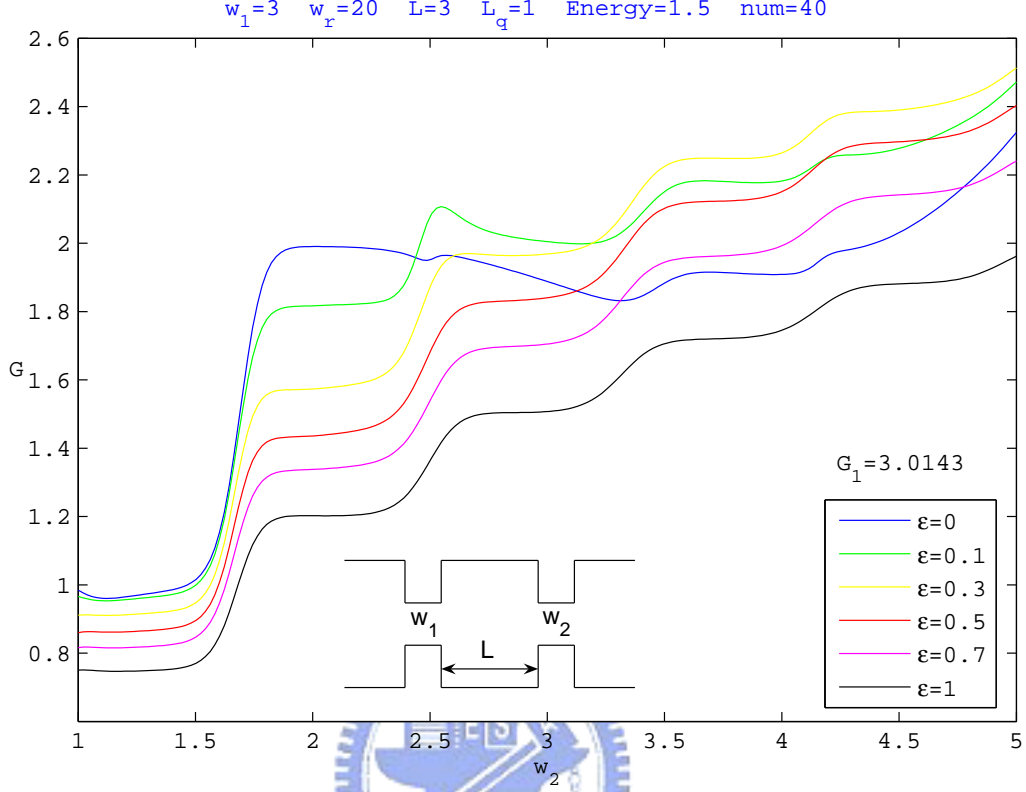


Figure 2.8: Total Conductance of two QPCs in series plotted against the width of QPC2. The width of QPC1 is fixed. L_q the length of QPC is $1 \times \frac{1}{k_f} = 9.2$ nm and they are separated with $L = 3 \times \frac{1}{k_f} = 27.6$ nm. ϵ is decoherence strength. Energy of incident electron is 1.5 with unit $E^* = \frac{\hbar^2 \pi^2 k_F^2}{2m^*}$ eV. Number of subband is 40 in our approximation.

In classical mechanics, we can regard QPC as a type of resistance. And the effect of decoherence is more probably happened between the QPC1 and QPC2. If two QPCs in series can be regarded as two resistance in series. Therefore, the conductance has relationship $\frac{1}{G_{total}} = \frac{1}{G_1} + \frac{1}{G_2}$. Via this formula we can obtain Fig. 2.9 (Conductance of QPC2 plotted against its width). In this point of view, we can see the effect of decoherence between double QPCs in series. When decoherence strength ϵ is 1, conductance of QPC2 is quantized just like Fig. 2.7. It means these two QPCs can be regarded as two resistances in series under totally decoherent. If ϵ is much less than 1, the total conductance is strongly coupled in their phase difference under quantum mechanics. The interference effect will contribute extra conductance or resistance.

CHAPTER 2. DECOHERENCE EFFECT IN A SERIAL QUANTUM POINT CONTACT STRUCTURE

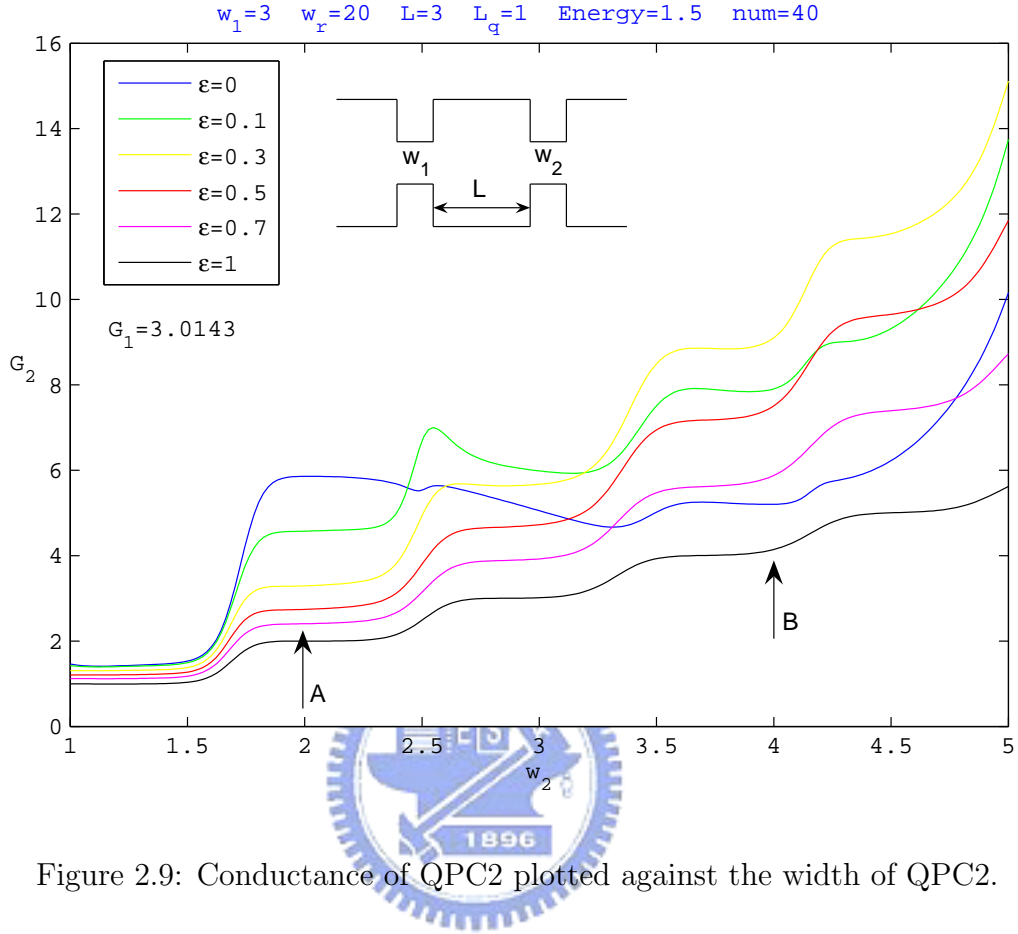


Figure 2.9: Conductance of QPC2 plotted against the width of QPC2.

When strength of decoherence ϵ is increasing, we observe conductance is decreasing in $w_2 = 2$ but increasing in $w_2 = 4$. This result gives us a hint: interference effect will raise conductance or lower conductance. If interference effect raise conductance, applying decoherence effect will lower conductance just like the case $w_2 = 2$. In $w_2 = 4$, conductance is raised when we give small decoherence effect, and lowered when we give more decoherence effect.

CHAPTER 2. DECOHERENCE EFFECT IN A SERIAL QUANTUM POINT CONTACT STRUCTURE

First, we want to know the physical reason make the difference in w_2 and w_4 . We know in open quantum dot, quasi-bound state would be lower than that in closed quantum dot. Conductance in different structure will give different behavior at the same energy. In order to observe the phenomenon, we make Fig. 2.10 and Fig. 2.11 to observe what happen in these two kind of case.

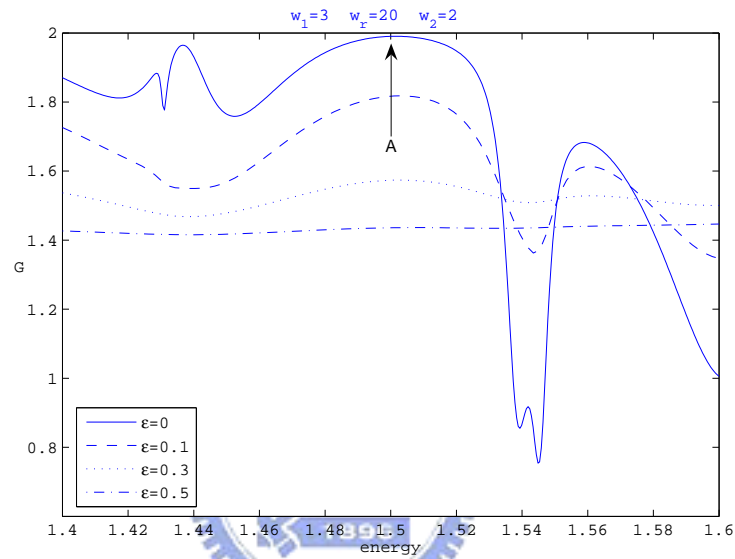


Figure 2.10: Total conductance plotted against incident energy under $w_2 = 2$.

In Fig. 2.10, it represents total conductance plotted against incident energy under $w_2 = 2$. There is an energy peak in $E = 1.5$

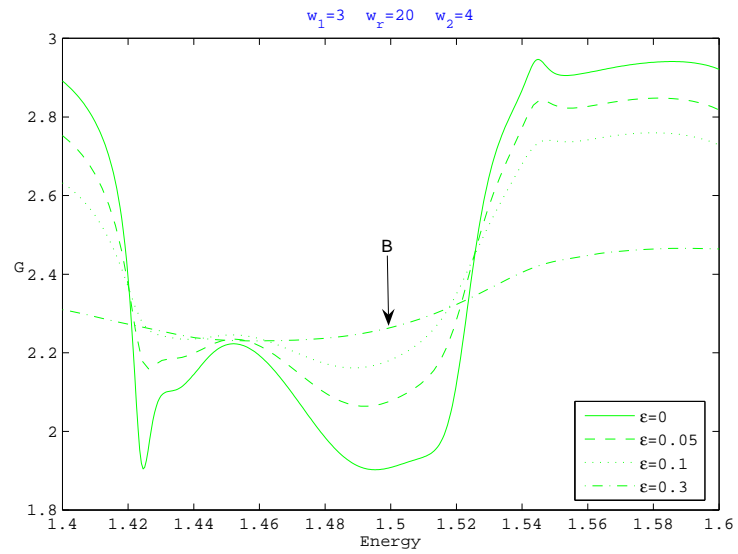


Figure 2.11: Total conductance plotted against incident energy under $w_2 = 4$.

In Fig. 2.11, it represents total conductance plotted against incident energy under $w_2 = 4$. There is an energy dip in $E = 1.5$. The resonance occurs in Fig. 2.11 so we can find out dip structure in it. Fig. 2.10 is the normal case.

Chapter 3

Quantum transport through a Rashba-type spin-orbit open quantum dot: in the absence of subband mixing



We consider an open quantum dot connected via two leads to the source and drain electrode as shown in figure 2-1. The lead has both Dresselhaus and Rashba spin-orbit interaction while the open quantum dot has only Rashba (SOI). In this chapter, we neglect subband-mixing to get analytic solution.

3.1 Solving the eigen state in channel with Dresselhaus and Rashba spin-orbit interaction in the absence of subband mixing

At first, we solve eigen wave function in lead with Dresselhaus and Rashba spin-orbit interaction. Hamiltonian of Rashba spin-orbit interaction is

$$\mathcal{H}_R = \frac{\alpha}{\hbar} (p_x \sigma_y - p_y \sigma_x) \quad (3.1)$$

Hamiltonian of Dresselhaus spin-orbit interaction is

$$\mathcal{H}_D = \frac{\beta}{\hbar} (p_x \sigma_x - p_y \sigma_y) \quad (3.2)$$

We assume the Dresselhaus and Rashba coefficient are the same $\alpha = \beta$ in the lead. The lead is very narrow so we can neglect the subband mixing in lead. Therefore, Hamiltonian in the lead can be written as:

$$H = -\frac{\hbar^2 \cdot \nabla^2}{2m} + V_c(x, y) - i\hbar \cdot \alpha_1 \frac{\partial}{\partial x} (\sigma_x + \sigma_y) \quad (3.3)$$

Here, the σ are the Pauli matrices and $V_c(x, y)$ is confining potential. Next, We choose our dimensionless unit as energy unit be $E^* = \frac{\hbar^2 k_F^2}{2m^*}$, length unit is $a^* = \frac{1}{k_F}$, and the unit of Rashba coefficient is $\frac{\hbar}{2m}$. So we get dimensionless Hamiltonian:

$$H = -\nabla^2 + V(x, y) - i \cdot \alpha_1 \frac{\partial}{\partial x} (\sigma_x + \sigma_y) \quad (3.4)$$

Its eigenstate is $\chi_{\pm} = \frac{1}{\sqrt{2}} \begin{pmatrix} 1 \\ \pm e^{i\frac{\pi}{4}} \end{pmatrix}$ with eigenvalue $\lambda = \pm\sqrt{2}$. For given eigenstate, we have our wave function $\psi_{L,\pm} \cdot \chi_{\pm}$. Wave function must satisfy boundary condition and be eigenfunction of Hamiltonian Equation.

$$-\nabla^2 \psi_{L,\pm} + V_c(x, y) \cdot \psi_{L,\pm} \mp i \cdot \sqrt{2} \cdot \alpha_1 \frac{\partial}{\partial x} \psi_{L,\pm} = E \cdot \psi_{L,\pm} \quad (3.5)$$

We consider confining potential is hard wall confinement. Therefore, the separation of variables is accomplished by the substitution: $\psi_{L,\pm} = \phi(x)_\pm \cdot \phi_n(y)$ and $E = E_{x,\pm} + \left(\frac{n\pi}{w_1}\right)^2$ where

$$\phi_n(y) = \sqrt{\frac{2}{w_1}} \cdot \sin \left[\frac{n\pi(y-d)}{w_1} \right] \quad (3.6)$$

In the usual way, we find separate equations for $\phi(x)_\pm$

$$\left[-i \frac{\partial}{\partial x} \pm \frac{\alpha_1}{\sqrt{2}} \right]^2 \cdot \phi(x)_\pm - \frac{\alpha_1^2}{2} \cdot \phi(x)_\pm = E_{x,\pm} \cdot \phi(x)_\pm \quad (3.7)$$

Assume $\phi(x) = e^{\mp i \frac{\alpha_1}{\sqrt{2}} x} \cdot \varphi(x)_\pm$ to simplify this differential equation.

$$-\frac{\partial^2}{\partial x^2} \varphi(x)_\pm = \left(E_{x,\pm} + \frac{\alpha_1^2}{2} \right) \cdot \varphi(x)_\pm \quad (3.8)$$

The solution wave function in the lead is found to be:

$$\psi_L(x, y) = e^{ik_n x} \cdot e^{\mp i \frac{\alpha_1}{\sqrt{2}} x} \cdot \phi_n(y) \cdot \chi_\pm \quad (3.9)$$

$$k_n = \sqrt{\varepsilon - \left(\frac{n\pi}{w_1}\right)^2 + \frac{\alpha_1^2}{2}} \quad (3.10)$$

After solving eigen state in the lead, dimensionless Hamiltonian in the dot can be written as:

$$\begin{aligned}
 H &= -\nabla^2 + V(x, y) + \alpha_2 \cdot (\vec{p} \times \hat{z}) \cdot \vec{\sigma} \\
 &= -\nabla^2 + V(x, y) - i \cdot \alpha_2 \frac{\partial}{\partial x} \sigma_y
 \end{aligned} \tag{3.11}$$

We neglect subband mixing term $+i \frac{\partial}{\partial y} \sigma_x$ in Hamiltonian. In fact, this way didn't work for our model physically. But its solution is analytic form to give us a hint to real case.

We also have spin eigenstate $\sigma_{\pm} = \frac{1}{\sqrt{2}} \begin{pmatrix} 1 \\ \pm i \end{pmatrix}$ with eigenvalue $\lambda = \pm 1$. Then the same algebra process as lead, we can get dispersion relation $E = E_{x,\pm} + \left(\frac{n\pi}{w_2}\right)^2$ and total wave function $\psi_{2,\pm} = \phi(x)_{\pm} \cdot \tilde{\phi}(y)$. where

$$\tilde{\phi}(y) = \sqrt{\frac{2}{w_2}} \cdot \sin\left(\frac{n\pi y}{w_2}\right) \tag{3.12}$$

As the same process in previous section, we can obtain x -direction differential equation.

$$\left[-i \frac{\partial}{\partial x} \pm \frac{\alpha_2}{2} \right]^2 \cdot \tilde{\phi}(x)_{\pm} - \frac{\alpha_2^2}{4} \cdot \tilde{\phi}(x)_{\pm} = E_{x,\pm} \cdot \tilde{\phi}(x)_{\pm} \tag{3.13}$$

The solution wave function in the lead is found to be:

$$\psi_D = e^{\mp i \frac{\alpha_2}{2} x} \cdot e^{i \tilde{k}_n x} \cdot \tilde{\phi}_n(y) \cdot \sigma_{\pm} \tag{3.14}$$

$$\tilde{k}_n = \sqrt{\varepsilon - \left(\frac{n\pi}{W_1}\right)^2 + \frac{\alpha_2^2}{4}} \tag{3.15}$$

3.2 Matching boundary condition and scattering method

We can take the solution to be of the form:

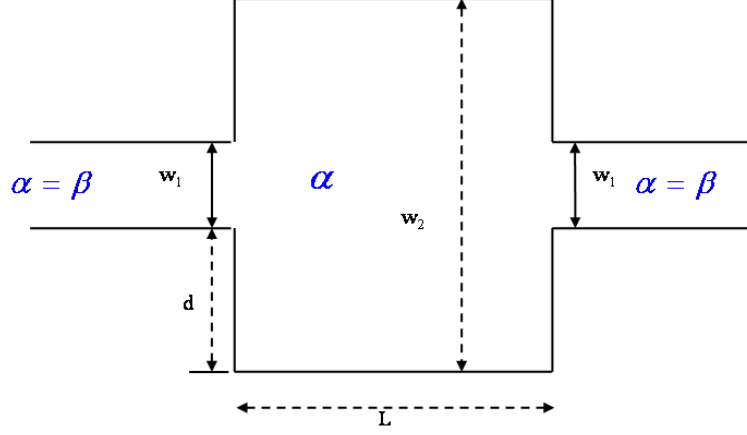


Figure 3.1: The model of Rashba-type spin-orbit open quantum dot

if $d < y < d + w_1$ and $x < 0$

$$\begin{aligned} \psi_{L1}(x, y) = & e^{ik_{n_0}x} \cdot e^{-i\frac{\alpha_1}{\sqrt{2}}x} \cdot \phi_{n_0}(y) \cdot \chi_+ \\ & + \sum_n \left[r_{n,+} \cdot e^{-ik_nx} \cdot e^{-i\frac{\alpha_1}{\sqrt{2}}x} \cdot \phi_n(y) \cdot \chi_+ + r_{n,-} \cdot e^{-ik_nx} \cdot e^{+i\frac{\alpha_1}{\sqrt{2}}x} \cdot \phi_n(y) \cdot \chi_- \right] \end{aligned} \quad (3.16)$$

if $0 < y < w_2$ and $0 < x < L$

$$\begin{aligned} \psi_D = & \sum_n \left[A_{n,+} \cdot e^{-i\frac{\alpha_2}{2}x} \cdot e^{i\tilde{k}_nx} \cdot \tilde{\phi}_n(y) \cdot \sigma_+ + A_{n,-} \cdot e^{+i\frac{\alpha_2}{2}x} \cdot e^{i\tilde{k}_nx} \cdot \tilde{\phi}_n(y) \cdot \sigma_- \right] \\ & + \sum_n \left[B_{n,+} \cdot e^{-i\frac{\alpha_2}{2}x} \cdot e^{-i\tilde{k}_nx} \cdot \tilde{\phi}_n(y) \cdot \sigma_+ + B_{n,-} \cdot e^{+i\frac{\alpha_2}{2}x} \cdot e^{-i\tilde{k}_nx} \cdot \tilde{\phi}_n(y) \cdot \sigma_- \right] \end{aligned} \quad (3.17)$$

if $d < y < d + w_1$ and $x > L$

$$\psi_{L2}(x, y) = \sum_n \left[t_{n,+} \cdot e^{ik_nx} \cdot e^{-i\frac{\alpha_1}{\sqrt{2}}x} \cdot \phi_n(y) \cdot \chi_+ + t_{n,-} \cdot e^{ik_nx} \cdot e^{+i\frac{\alpha_1}{\sqrt{2}}x} \cdot \phi_n(y) \cdot \chi_- \right] \quad (3.18)$$

Match wave function continuous at $x = 0$:

$$\begin{aligned} & \phi_{n_0}(y) \cdot \chi_+ + \sum_n [r_{n,+} \cdot \chi_+ + r_{n,-} \cdot \chi_-] \cdot \phi_n(y) \\ &= \sum_n [A_{n,+} \cdot \sigma_+ + A_{n,-} \cdot \sigma_- + B_{n,+} \cdot \sigma_+ + B_{n,-} \cdot \sigma_-] \cdot \tilde{\phi}_n(y) \end{aligned} \quad (3.19)$$

Multiplying Eq. (3.19) by $\sigma_{\pm}^* \cdot \int_d^{d+w_1} \tilde{\phi}_{n'}(y) dy$, we obtain

$$\begin{aligned} & (\sigma_+^* \cdot \chi_+) \cdot \int_d^{d+w_1} \tilde{\phi}_{n'}(y) \cdot \phi_{n_0}(y) dy \\ &+ \sum_n [r_{n,+} \cdot (\sigma_+^* \cdot \chi_+) + r_{n,-} \cdot (\sigma_+^* \cdot \chi_-)] \cdot \int_d^{d+w_1} \tilde{\phi}_{n'}(y) \cdot \phi_n(y) dy \\ &= \sum_n [A_{n,+} \cdot \delta_{n',n} + B_{n,+} \cdot \delta_{n',n}] \end{aligned} \quad (3.20)$$

$$\begin{aligned} & (\sigma_-^* \cdot \chi_+) \cdot \int_d^{d+w_1} \tilde{\phi}_{n'}(y) \cdot \phi_{n_0}(y) dy \\ &+ \sum_n [r_{n,+} \cdot (\sigma_-^* \cdot \chi_+) + r_{n,-} \cdot (\sigma_-^* \cdot \chi_-)] \cdot \int_d^{d+w_1} \tilde{\phi}_{n'}(y) \cdot \phi_n(y) dy \\ &= \sum_n [A_{n,-} \cdot \delta_{n',n} + B_{n,-} \cdot \delta_{n',n}] \end{aligned} \quad (3.21)$$

Match slope of wave function continuous at $x = 0$. In the boundary, we must input step function in our Hamiltonian. Besides, we must keep our Hamiltonian be hermitian operator.

$$\begin{aligned} H &= -\nabla^2 + V(x, y) + \alpha_1 \left(-i \frac{\partial}{\partial x} + i \frac{\partial}{\partial y} \right) (\sigma_x + \sigma_y) \\ &+ \frac{1}{2} \theta(x) \cdot \left[-i \cdot \alpha_2 \frac{\partial}{\partial x} \sigma_y - \alpha_1 \left(-i \frac{\partial}{\partial x} + i \frac{\partial}{\partial y} \right) (\sigma_x + \sigma_y) \right] \\ &+ \frac{1}{2} \left[-i \cdot \alpha_2 \frac{\partial}{\partial x} \sigma_y - \alpha_1 \left(-i \frac{\partial}{\partial x} + i \frac{\partial}{\partial y} \right) (\sigma_x + \sigma_y) \right] \cdot \theta(x) \end{aligned} \quad (3.22)$$

Put this Hamiltonian into $\int_{0-\varepsilon}^{0+\varepsilon} H \cdot \psi = 0$ to match differential boundary condition. we obtain

$$-\left(\frac{\partial}{\partial x} + \frac{1}{2}i \cdot \alpha_2 \cdot \sigma_y\right) \cdot \psi|_{0+\varepsilon} + \left[\frac{\partial}{\partial x} + \frac{1}{2}i \cdot \alpha_1 \cdot (\sigma_x + \sigma_y)\right] \cdot \psi|_{0-\varepsilon} = 0 \quad (3.23)$$

Substituting Eq. (4.42) by Eq. (3.16) and Eq. (3.17)

$$\begin{aligned} & k_{n_0} \cdot \phi_{n_0}(y) \cdot \chi_+ - \sum_n [r_{n,+} \cdot \chi_+ + r_{n,-} \cdot \chi_-] \cdot k_n \cdot \phi_n(y) \\ &= \sum_n [A_{n,+} \cdot \sigma_+ + A_{n,-} \cdot \sigma_- - B_{n,+} \cdot \sigma_+ - B_{n,-} \cdot \sigma_-] \cdot \tilde{k}_n \cdot \tilde{\phi}_n(y) \end{aligned} \quad (3.24)$$

Multiplying Eq. (4.43) by $\chi_{\pm}^* \cdot \int_d^{d+w_1} \phi_{n'}(y) dy$, we obtain

$$\begin{aligned} & k_{n_0} \cdot \delta_{n',n_0} + \sum_n r_{n,+} \cdot (-k_n) \cdot \delta_{n',n} \\ &= \sum_n [A_{n,+} \cdot (\chi_+^* \cdot \sigma_+) + A_{n,-} \cdot (\chi_+^* \cdot \sigma_-) - B_{n,+} \cdot (\chi_+^* \cdot \sigma_+) - B_{n,-} \cdot (\chi_+^* \cdot \sigma_-)] \\ & \quad \times \int_d^{d+w_1} \tilde{k}_n \cdot \phi_{n'}(y) \cdot \tilde{\phi}_n(y) dy \end{aligned} \quad (3.25)$$

$$\begin{aligned} & \sum_n r_{n,-} \cdot (-k_n) \cdot \delta_{n',n} \\ &= \sum_n [A_{n,+} \cdot (\chi_-^* \cdot \sigma_+) + A_{n,-} \cdot (\chi_-^* \cdot \sigma_-) - B_{n,+} \cdot (\chi_-^* \cdot \sigma_+) - B_{n,-} \cdot (\chi_-^* \cdot \sigma_-)] \\ & \quad \times \int_d^{d+w_1} \tilde{k}_n \cdot \phi_{n'}(y) \cdot \tilde{\phi}_n(y) dy \end{aligned} \quad (3.26)$$

Therefore, we can write down the matrix equation at the boundary $x = 0$.

$$\begin{bmatrix} M_{11} & M_{12} & M_{13} & M_{14} \\ M_{21} & M_{22} & M_{23} & M_{24} \\ M_{31} & M_{32} & M_{33} & M_{34} \\ M_{41} & M_{42} & M_{43} & M_{44} \end{bmatrix} \cdot \begin{bmatrix} \delta_{n,n_0} \\ 0 \\ r_{n,+} \\ r_{n,-} \end{bmatrix} = \begin{bmatrix} N_{11} & N_{12} & N_{13} & N_{14} \\ N_{21} & N_{22} & N_{23} & N_{24} \\ N_{31} & N_{32} & N_{33} & N_{34} \\ N_{41} & N_{42} & N_{43} & N_{44} \end{bmatrix} \cdot \begin{bmatrix} A_{n,+} \\ A_{n,-} \\ B_{n,+} \\ B_{n,-} \end{bmatrix} \quad (3.27)$$

Following the same process, match wave function continuous at $x = L$:

$$\begin{aligned} & \sum_n \left[A_{n,+} \cdot e^{-i\frac{\alpha_2}{2}L} \cdot \sigma_+ + A_{n,-} \cdot e^{+i\frac{\alpha_2}{2}L} \cdot \sigma_- \right] \cdot e^{i\tilde{k}_n L} \cdot \tilde{\phi}_n(y) \\ & + \sum_n \left[B_{n,+} \cdot e^{-i\frac{\alpha_2}{2}L} \cdot \sigma_+ + B_{n,-} \cdot e^{+i\frac{\alpha_2}{2}L} \cdot \sigma_- \right] \cdot e^{-i\tilde{k}_n L} \cdot \tilde{\phi}_n(y) \\ & = \sum_n \left[t_{n,+} \cdot e^{-i\frac{\alpha_1}{\sqrt{2}}L} \cdot \chi_+ + t_{n,-} \cdot e^{+i\frac{\alpha_1}{\sqrt{2}}L} \cdot \chi_- \right] \cdot e^{ik_n L} \cdot \phi_n(y) \end{aligned} \quad (3.28)$$

Multiplying Eq. (4.32) by $\sigma_{\pm}^* \cdot \int_d^{d+w_1} \tilde{\phi}_{n'}(y) dy$, we obtain

$$\begin{aligned} & \sum_n \left[A_{n,+} \cdot e^{i\tilde{k}_n L} + B_{n,+} \cdot e^{-i\tilde{k}_n L} \right] \cdot e^{-i\frac{\alpha_2}{2}L} \cdot \delta_{n',n} \\ & = \sum_n \left[t_{n,+} \cdot e^{-i\frac{\alpha_1}{\sqrt{2}}L} \cdot (\sigma_+^* \cdot \chi_+) + t_{n,-} \cdot e^{+i\frac{\alpha_1}{\sqrt{2}}L} \cdot (\sigma_+^* \cdot \chi_-) \right] \\ & \quad \times e^{ik_n L} \cdot \int_d^{d+w_1} \tilde{\phi}_{n'}(y) \cdot \phi_n(y) dy \end{aligned} \quad (3.29)$$

$$\begin{aligned} & \sum_n \left[A_{n,-} \cdot e^{i\tilde{k}_n L} + B_{n,-} \cdot e^{-i\tilde{k}_n L} \right] \cdot e^{+i\frac{\alpha_2}{2}L} \cdot \delta_{n',n} \\ & = \sum_n \left[t_{n,+} \cdot e^{-i\frac{\alpha_1}{\sqrt{2}}L} \cdot (\sigma_-^* \cdot \chi_+) + t_{n,-} \cdot e^{+i\frac{\alpha_1}{\sqrt{2}}L} \cdot (\sigma_-^* \cdot \chi_-) \right] \\ & \quad \times e^{ik_n L} \cdot \int_d^{d+w_1} \tilde{\phi}_{n'}(y) \cdot \phi_n(y) dy \end{aligned} \quad (3.30)$$

Match slope of wave function continuous at $x = L$. We also must input step function in our Hamiltonian and keep it be hermitian operator.

$$\begin{aligned}
 & \sum_n \left[A_{n,+} \cdot e^{-i\frac{\alpha_2}{2}L} \cdot \sigma_+ + A_{n,-} \cdot e^{+i\frac{\alpha_2}{2}L} \cdot \sigma_- \right] \cdot \tilde{k}_n \cdot e^{i\tilde{k}_n L} \cdot \tilde{\phi}_n(y) \\
 - & \sum_n \left[B_{n,+} \cdot e^{-i\frac{\alpha_2}{2}L} \cdot \sigma_+ + B_{n,-} \cdot e^{+i\frac{\alpha_2}{2}L} \cdot \sigma_- \right] \cdot \tilde{k}_n \cdot e^{-i\tilde{k}_n L} \cdot \tilde{\phi}_n(y) \\
 = & \sum_n \left[t_{n,+} \cdot e^{-i\frac{\alpha_1}{\sqrt{2}}L} \cdot \chi_+ + t_{n,-} \cdot e^{+i\frac{\alpha_1}{\sqrt{2}}L} \cdot \chi_- \right] \cdot k_n \cdot e^{i k_n L} \cdot \phi_n(y) \tag{3.31}
 \end{aligned}$$

Multiplying Eq. (4.37) by $\chi_{\pm}^* \cdot \int_d^{d+w_1} \phi_{n'}(y) dy$, we obtain

$$\begin{aligned}
 & \sum_n \left[A_{n,+} \cdot e^{-i\frac{\alpha_2}{2}L} \cdot \langle \chi_+ | \sigma_+ \rangle + A_{n,-} \cdot e^{+i\frac{\alpha_2}{2}L} \cdot \langle \chi_+ | \sigma_- \rangle \right] \\
 & \times \tilde{k}_n \cdot e^{i\tilde{k}_n L} \cdot \int_d^{d+w_1} \phi_{n'}(y) \cdot \tilde{\phi}_n(y) dy \\
 - & \sum_n \tilde{k}_n \cdot e^{-i\tilde{k}_n L} \cdot \left[B_{n,+} \cdot e^{-i\frac{\alpha_2}{2}L} \cdot \langle \chi_+ | \sigma_+ \rangle + B_{n,-} \cdot e^{+i\frac{\alpha_2}{2}L} \cdot \langle \chi_+ | \sigma_- \rangle \right] \\
 & \times \tilde{k}_n \cdot e^{-i\tilde{k}_n L} \int_d^{d+w_1} \phi_{n'}(y) \cdot \tilde{\phi}_n(y) dy \\
 = & \sum_n \left[t_{n,+} \cdot k_n \cdot e^{i k_n L} \cdot e^{-i\frac{\alpha_1}{\sqrt{2}}L} \cdot \delta_{n',n} \right] \tag{3.32}
 \end{aligned}$$

$$\begin{aligned}
 & \sum_n \left[A_{n,+} \cdot e^{-i\frac{\alpha_2}{2}L} \cdot \langle \chi_- | \sigma_+ \rangle + A_{n,-} \cdot e^{+i\frac{\alpha_2}{2}L} \cdot \langle \chi_- | \sigma_- \rangle \right] \\
 & \times \tilde{k}_n \cdot e^{i\tilde{k}_n L} \cdot \int_d^{d+w_1} \phi_{n'}(y) \cdot \tilde{\phi}_n(y) dy \\
 - & \sum_n \left[B_{n,+} \cdot e^{-i\frac{\alpha_2}{2}L} \cdot \langle \chi_- | \sigma_+ \rangle + B_{n,-} \cdot e^{+i\frac{\alpha_2}{2}L} \cdot \langle \chi_- | \sigma_- \rangle \right] \\
 & \times \tilde{k}_n \cdot e^{-i\tilde{k}_n L} \cdot \int_d^{d+w_1} \phi_{n'}(y) \cdot \tilde{\phi}_n(y) dy \\
 = & \sum_n \left[t_{n,-} \cdot k_n \cdot e^{i k_n L} \cdot e^{+i\frac{\alpha_1}{\sqrt{2}}L} \cdot \delta_{n',n} \right] \tag{3.33}
 \end{aligned}$$

CHAPTER 3. QUANTUM TRANSPORT THROUGH A RASHBA-TYPE
SPIN-ORBIT OPEN QUANTUM DOT: IN THE ABSENCE OF SUBBAND MIXING

Therefore, we can write down the matrix equation at the boundary $x = L$.

$$\begin{bmatrix} P_{11} & P_{12} & P_{13} & P_{14} \\ P_{21} & P_{22} & P_{23} & P_{24} \\ P_{31} & P_{32} & P_{33} & P_{34} \\ P_{41} & P_{42} & P_{43} & P_{44} \end{bmatrix} \cdot \begin{bmatrix} A_{n,+} \\ A_{n,-} \\ B_{n,+} \\ B_{n,-} \end{bmatrix} = \begin{bmatrix} Q_{11} & Q_{12} & Q_{13} & Q_{14} \\ Q_{21} & Q_{22} & Q_{23} & Q_{24} \\ Q_{31} & Q_{32} & Q_{33} & Q_{34} \\ Q_{41} & Q_{42} & Q_{43} & Q_{44} \end{bmatrix} \cdot \begin{bmatrix} t_{n,+} \\ t_{n,-} \\ 0 \\ 0 \end{bmatrix} \quad (3.34)$$

Then we combine matrix equation Eq. (3.27) and Eq. (3.27), we can obtain transfer matrix defined by

$$T \cdot \begin{bmatrix} \delta_{n,n_0} \\ 0 \\ r_{n,+} \\ r_{n,-} \end{bmatrix} = \begin{bmatrix} t_{n,+} \\ t_{n,-} \\ 0 \\ 0 \end{bmatrix} \quad (3.35)$$


Then we have:

$$T = (Q)^{-1} \cdot P \cdot (N)^{-1} \cdot M = \begin{bmatrix} T_{11} & T_{12} \\ T_{21} & T_{22} \end{bmatrix} \quad (3.36)$$

and

$$\begin{aligned} T_{11} \cdot \begin{bmatrix} \delta_{n,n_0} \\ 0 \end{bmatrix} + T_{12} \cdot \begin{bmatrix} r_{n,+} \\ r_{n,-} \end{bmatrix} &= \begin{bmatrix} t_{n,+} \\ t_{n,-} \end{bmatrix} \\ T_{21} \cdot \begin{bmatrix} \delta_{n,n_0} \\ 0 \end{bmatrix} + T_{22} \cdot \begin{bmatrix} r_{n,+} \\ r_{n,-} \end{bmatrix} &= 0 \end{aligned} \quad (3.37)$$

3.3 Numerical result and discussion

In this section, we show the numerical results and discussion of open quantum dot with spin-orbit interaction but neglect the subband mixing. Length unit is $\frac{1}{k_f}=4$ nm and energy unit is $E^* = \frac{\hbar^2 k_F^2}{2m^*} = 0.059$ eV. Where $k_f = \sqrt{2\pi n} = 2.5 \times 10^8$ (1/m) in InGaAs.

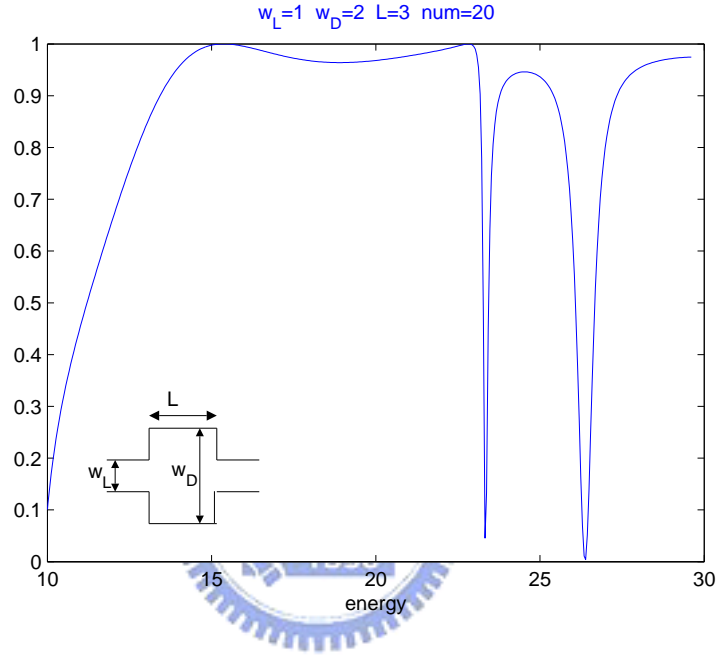


Figure 3.2: Open quantum dot in the absence of spin-orbit interaction

Fig. 3.2 shows the transmission plotted against incident energy in open quantum dot in the absence of spin-orbit interaction. In order to simplify our calculation, we let our case is symmetric in transverse direction. W_L represents the width of lead and W_D is the width of dot. len is the length of open quantum dot. Number of subband in calculation is 20. This figure help us to realize what happens in spin-orbit interaction. Dot vertical line represents the eigen energy of quasi-bound state. We find that whenever incident energy aligns with particle-in-a-box energy levels, there are dramatic changes in G (i.e the resonant energy). Surprisingly, this is a system with large opening of W_D/W_L ratio equal to 2. It is hardly a close box although the resonant states and particle-in-a-box states match so well. Wave fuction (n_x, n_y) states for particle-in-a-box (or a closed dot) is

$$\psi_{n_x, n_y}(x, y) = \sin\left(\frac{n_x \pi}{L} x\right) \sin\left(\frac{n_y \pi}{W_D} y\right) \quad (3.38)$$

We observe that whenever particle-in-a-box states (n_x, n_y) ; $n_y = 1$, the correspondence resonant energy does not form a quasi-bound state. Although we cannot explain the selection rules of the formation of quasi-bound state in the dot yet, we are able to describe the behavior of electron whenever its incident energy coincides with energy level of particle-in-a-box. We find that wave function do not build up in the dot for $n_y=1$ by plotting its time averaged probability density. But for $(n_y=3)$ states, wave function build up inside the dot for its correspondence incident energy. Note that, for particle-in-a-box states of $(n_y=2)$, because in symmetric structure, wave function coupling of odd and even is zero. We can get this conclusion by comparing Fig. 3.3 and Fig. 3.4.

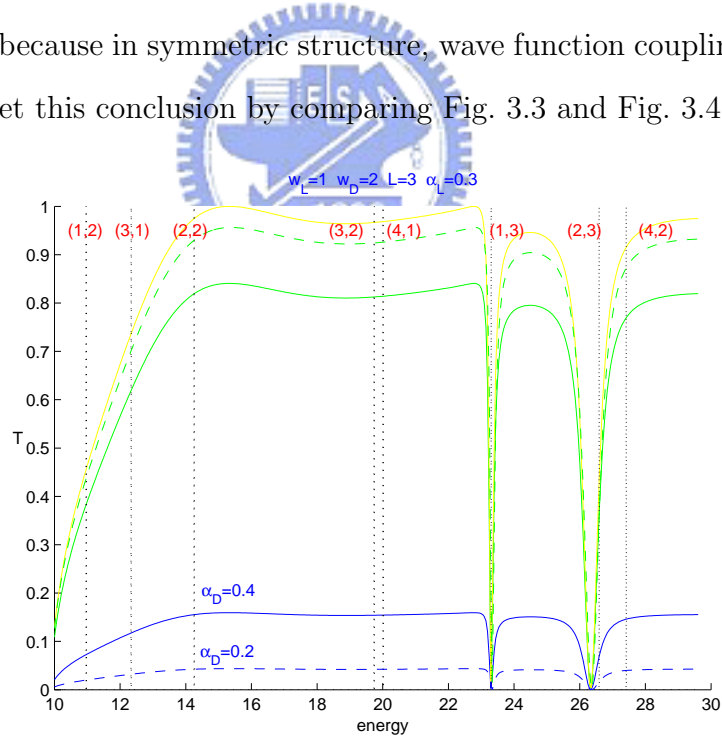


Figure 3.3: Open quantum dot with spin-orbit interaction in absence of subband mixing

CHAPTER 3. QUANTUM TRANSPORT THROUGH A RASHBA-TYPE SPIN-ORBIT OPEN QUANTUM DOT: IN THE ABSENCE OF SUBBAND MIXING

In Fig. 3.3, Rashba effect in the open quantum dot will flip the spin. Total current doesn't make change in spin-orbit interaction. The stronger Rashba effect in the open quantum dot we have, the more spin flip. The flip ratio is only depend on the Rashba effect in the open quantum dot but independent of incident energy. And the ratio is independent of the Rashba and Dresselhaus effect in the lead, too.

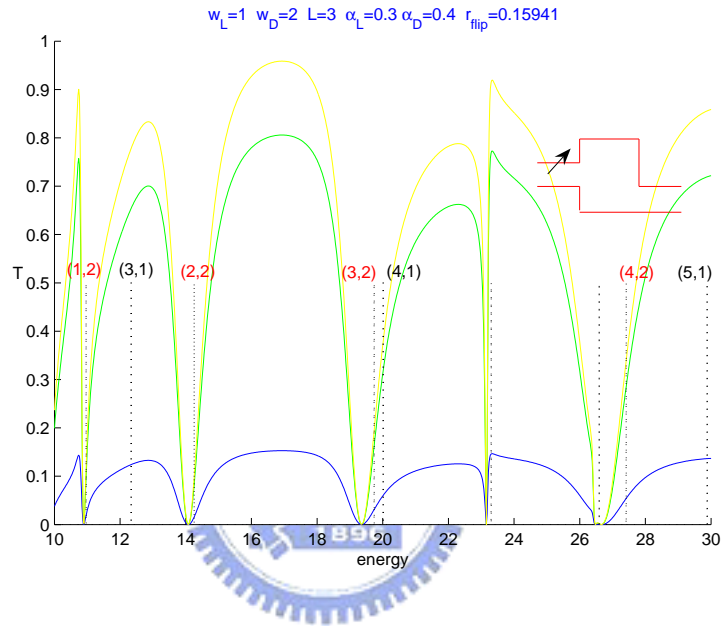


Figure 3.4: Open quantum dot with spin-orbit interaction in absence of subband mixing and asymmetric structure.

The same phenomenon we observe in asymmetric structure. Except the resonance structure due to wave function coupling of odd and even, the ratio of spin flipping is not influenced by asymmetric structure. And transmission is spin independent.

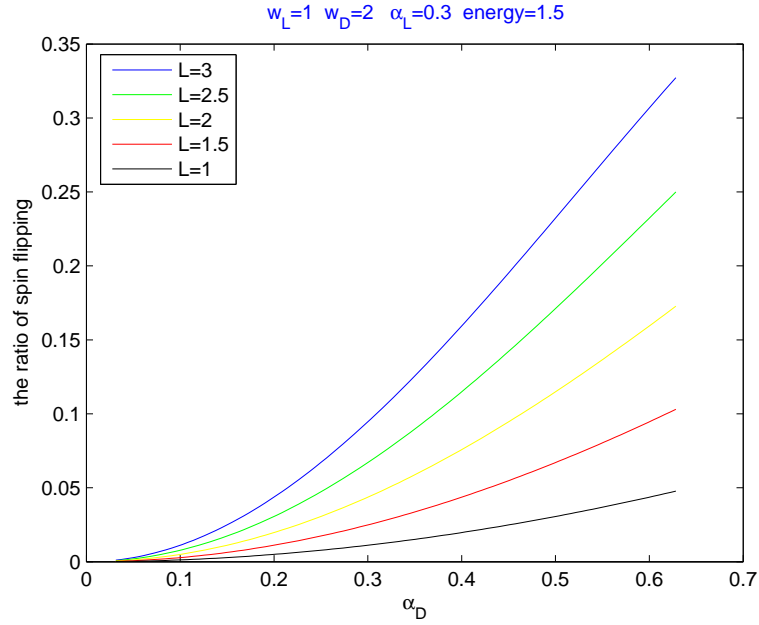


Figure 3.5: the ratio of flipping spin plotted against the rashba coupling in the open quantum dot.

Fig. 3.5 show that the ratio of flipping spin plotted against the Rashba coupling in open quantum dot. The ratio of flipping spin is defined by $T_{flipping}/T_{total}$. Note that the spin injection direction didn't influence the total transmission. It is because neglecting the subband mixing, it means we drop the possibility the spin precession at the same time. Surprisingly, this ratio is independent of incident energy, too. But we also can get a hint from these result, Rashba coupling in open quantum dot indeed influence the spin flipping. It is because that spin direction independent of momentum if we neglect the subband mixing at all.

Next chapter, we will take subband mixing into our consideration.

Chapter 4

Quantum transport through a Rashba-type spin-orbit open quantum dot: including subband mixing



4.1 Solving the eigen state in channel with Dresselhaus and Rashba spin-orbit interaction including subband mixing

In the previous section, we neglect the term to simplify our problem to get analytic form. In this section, we introduce a numerical method to get approximate solution. First, we must find proper basis function to span the eigen function in the open quantum dot.

Assume $\psi = e^{i(k_x x + k_y y)} \cdot \begin{pmatrix} a \\ b \end{pmatrix}$

Our Hamiltonian is:

$$H_D = -\nabla^2 + V(x, y) - \alpha \cdot \left(-i \frac{\partial}{\partial x} \sigma_y + i \frac{\partial}{\partial y} \sigma_x \right) \quad (4.1)$$

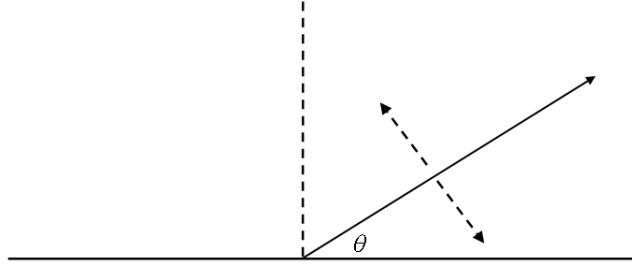


Figure 4.1: Assume a plain wave propagating in angle of θ

We want do fourier transform in our Hamiltonian and get numerical solution.

$$H \cdot \psi = [(k_x^2 + k_y^2) + \alpha \cdot (-k_x \cdot \sigma_y + k_y \cdot \sigma_x)] \cdot \psi = E \cdot \psi \quad (4.2)$$

Rewrite equation Eq. (4.2) into matrix form by following substitution $\sigma_x = \begin{bmatrix} 0 & 1 \\ 1 & 0 \end{bmatrix}$

and $\sigma_y = \begin{bmatrix} 0 & -i \\ i & 0 \end{bmatrix}$. we have:

$$\begin{bmatrix} k_x^2 + k_y^2 - E & \alpha \cdot (i \cdot k_x + k_y) \\ \alpha \cdot (-i \cdot k_x + k_y) & k_x^2 + k_y^2 - E \end{bmatrix} \cdot \begin{bmatrix} a \\ b \end{bmatrix} = 0 \quad (4.3)$$

Solve this eigen value problem, we can get eigen energy and corresponding eigen vector:

$$E_{\pm} = (k_x^2 + k_y^2) \pm \alpha \cdot \sqrt{k_x^2 + k_y^2} \quad (4.4)$$

set $a = 1$, then

$$\begin{pmatrix} a \\ b \end{pmatrix}_{\pm} = \frac{1}{\sqrt{2}} \begin{pmatrix} 1 \\ \mp i \frac{k_x + i k_y}{\sqrt{k_x^2 + k_y^2}} \end{pmatrix} = \frac{1}{\sqrt{2}} \begin{pmatrix} 1 \\ \mp i \cdot e^{i\theta} \end{pmatrix} \quad (4.5)$$

where $\theta = \tan^{-1} \frac{k_y}{k_x}$

We try to find eigen function in the open quantum channel with Rashba effect. One given incident wave must have two reflected wave with different spin state in order to match boundary condition in y-direction. One reflected wave case:

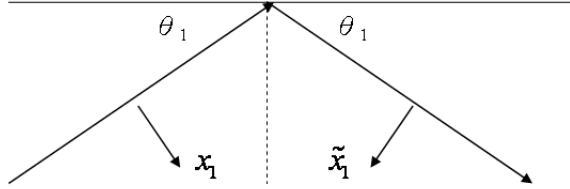


Figure 4.2: Assume one incident wave has one reflected wave

In order to keep conserve energy, reflected wave must have the same spin state as incident wave.

$$\psi_{inc} = e^{i(k_x x + k_y y)} \cdot \chi_1, \quad \chi_1 = \frac{1}{\sqrt{2}} \begin{pmatrix} 1 \\ -i \cdot e^{i\theta_1} \end{pmatrix} \quad (4.6)$$

$$\psi_{ref} = r \cdot e^{i(k_x x - k_y y)} \cdot \tilde{\chi}_1, \quad \tilde{\chi}_1 = \frac{1}{\sqrt{2}} \begin{pmatrix} 1 \\ -i \cdot e^{-i\theta_1} \end{pmatrix} \quad (4.7)$$

where $E_1 = k_x^2 + k_y^2 + \alpha \cdot \sqrt{k_x^2 + k_y^2}$. r is reflection coefficient, and we try to match boundary condition $y = 0$ to find proper r .

$$e^{ik_x x} \cdot \frac{1}{\sqrt{2}} \begin{pmatrix} 1 \\ -i \cdot e^{i\theta_1} \end{pmatrix} + r \cdot e^{ik_x x} \cdot \frac{1}{\sqrt{2}} \begin{pmatrix} 1 \\ -i \cdot e^{-i\theta_1} \end{pmatrix} = 0 \quad (4.8)$$

Each term in spin state can be separate:

$$\begin{cases} 1 + r = 0 \\ e^{i\theta_1} + r \cdot e^{-i\theta_1} = 0 \end{cases} \quad (4.9)$$

If $\theta_1 \neq 2n\pi$, no proper r can be found. To solve this problem, we must introduce another reflected wave with the same energy.

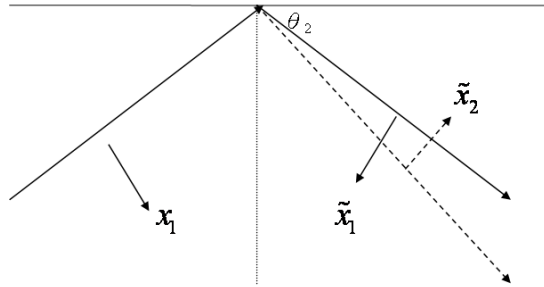


Figure 4.3: Add another reflected wave to fit boundary condition

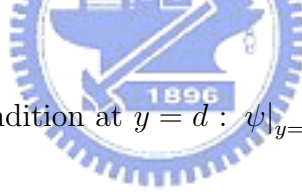
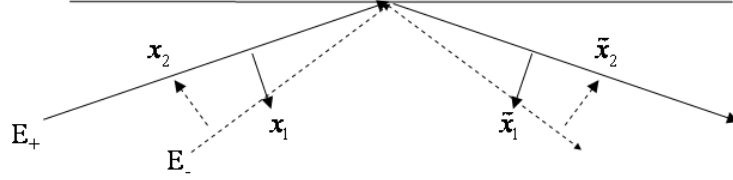
Let $\tilde{k} = \sqrt{k_x^2 + \tilde{k}_y^2}$ satisfy $k^2 - \alpha \cdot \tilde{k} = k^2 + \alpha \cdot k$ which $\tilde{k}_y > k_y$.

$$\psi_{total} = e^{i(k_x x + k_y y)} \cdot \chi_1 + r_{11} \cdot e^{i(k_x x - k_y y)} \cdot \tilde{\chi}_1 + r_{12} \cdot e^{i(k_x x - \tilde{k}_y y)} \cdot \tilde{\chi}_2 \quad (4.10)$$

As the same process, we have another incident wave:

$$\psi_{total} = e^{i(k_x x + \tilde{k}_y y)} \cdot \chi_2 + r_{21} \cdot e^{i(k_x x - k_y y)} \cdot \tilde{\chi}_1 + r_{22} \cdot e^{i(k_x x - k_y y)} \cdot \tilde{\chi}_2 \quad (4.11)$$

In a quantum channel with Rashba effect, wave function must satisfy boundary condition at $y = d$ and $y = 0$. So we calculate reflection coefficient r_{ij} and \tilde{r}_{ij} .



(1) Satisfied boundary condition at $y = d$: $\psi|_{y=d} = 0$

$$e^{ik_x x} \cdot e^{i\tilde{k}_y d} \cdot \begin{pmatrix} 1 \\ f_- \end{pmatrix} + \tilde{r}_{22} \cdot e^{ik_x x} \cdot e^{-i\tilde{k}_y d} \cdot \begin{pmatrix} 1 \\ h_- \end{pmatrix} + \tilde{r}_{21} \cdot e^{ik_x x} \cdot e^{-ik_y d} \cdot \begin{pmatrix} 1 \\ h_+ \end{pmatrix} = 0 \quad (4.12)$$

$$\begin{cases} e^{i\tilde{k}_y d} + \tilde{r}_{22} \cdot e^{-i\tilde{k}_y d} + \tilde{r}_{21} \cdot e^{-ik_y d} = 0 \\ e^{i\tilde{k}_y d} \cdot f_- + \tilde{r}_{22} \cdot e^{-i\tilde{k}_y d} \cdot h_- + \tilde{r}_{21} \cdot e^{-ik_y d} \cdot h_+ = 0 \end{cases} \quad (4.13)$$

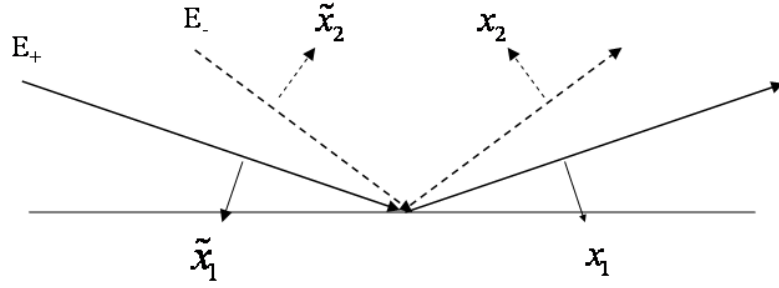
$$\tilde{r}_{22} = \frac{(-h_+ + f_-)}{(h_+ - h_-)} \cdot e^{i \cdot 2\tilde{k}_y d} \quad (4.14)$$

$$\tilde{r}_{21} = \frac{(-f_- + h_+)}{(h_+ - h_-)} \cdot e^{i \cdot (\tilde{k}_y + k_y) d} \quad (4.15)$$

Consider the other incident wave and following the same process, we obtain:

$$\tilde{r}_{12} = \frac{(-h_+ + f_+)}{(h_+ - h_-)} \cdot e^{i(\tilde{k}_y + k_y)d} \quad (4.16)$$

$$\tilde{r}_{11} = \frac{(-f_+ + h_-)}{(h_+ - h_-)} \cdot e^{i \cdot 2\tilde{k}_y d} \quad (4.17)$$



(2) Satisfied boundary condition at $y = 0$: $\psi|_{y=0} = 0$

$$e^{ik_{xx}} \cdot \begin{pmatrix} 1 \\ h_- \end{pmatrix} + r_{22} \cdot e^{ik_{xx}} \cdot \begin{pmatrix} 1 \\ f_- \end{pmatrix} + r_{21} \cdot e^{ik_{xx}} \cdot \begin{pmatrix} 1 \\ f_+ \end{pmatrix} = 0 \quad (4.18)$$

$$\begin{cases} 1 + r_{22} + r_{21} = 0 \\ h_- + r_{22} \cdot f_- + r_{21} \cdot f_+ = 0 \end{cases} \quad (4.19)$$

$$r_{22} = \frac{-f_+ + h_-}{f_+ - f_-} \quad (4.20)$$

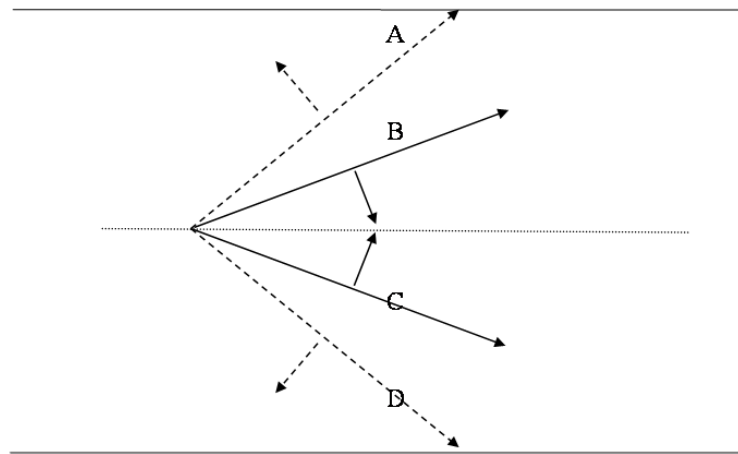
$$r_{21} = \frac{-h_- + f_+}{f_+ - f_-} \quad (4.21)$$

Consider the other incident wave and following the same process, we obtain:

$$r_{12} = \frac{-f_+ + h_+}{f_+ - f_-} \quad (4.22)$$

$$r_{11} = \frac{-h_+ + f_-}{f_+ - f_-} \quad (4.23)$$

Now, we can write down the eigen function in a quantum channel with Rashba effect by linear combination of four wave function which have the same energy.



4 component wave at the same energy:

$$A : e^{ik_x x} \cdot e^{i\tilde{k}_y y} \cdot \chi_2, \quad E = \tilde{k}^2 - \alpha \cdot \tilde{k}, \quad x_2 = \frac{1}{\sqrt{2}} \begin{pmatrix} 1 \\ i \cdot e^{i\theta_2} \end{pmatrix} \quad (4.24)$$

$$B : e^{ik_x x} \cdot e^{ik_y y} \cdot \chi_1, \quad E = k^2 + \alpha \cdot k, \quad x_1 = \frac{1}{\sqrt{2}} \begin{pmatrix} 1 \\ -i \cdot e^{i\theta_1} \end{pmatrix} \quad (4.25)$$

$$C : e^{ik_x x} \cdot e^{-ik_y y} \cdot \tilde{\chi}_1, \quad E = k^2 + \alpha \cdot k, \quad \tilde{x}_1 = \frac{1}{\sqrt{2}} \begin{pmatrix} 1 \\ -i \cdot e^{-i\theta_1} \end{pmatrix} \quad (4.26)$$

$$D : e^{ik_x x} \cdot e^{-i\tilde{k}_y y} \cdot \tilde{\chi}_2, \quad E = \tilde{k}^2 - \alpha \cdot \tilde{k}, \quad \tilde{x}_2 = \frac{1}{\sqrt{2}} \begin{pmatrix} 1 \\ i \cdot e^{-i\theta_2} \end{pmatrix} \quad (4.27)$$

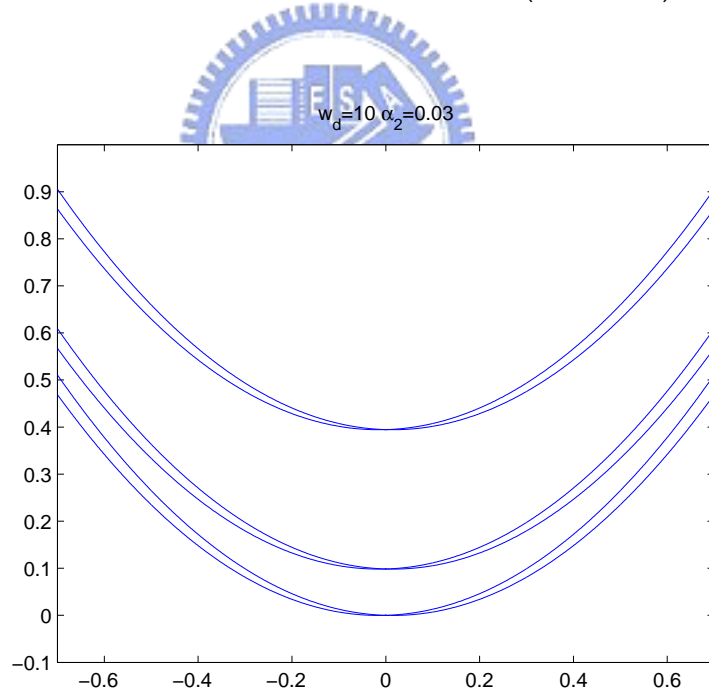


Figure 4.4: Dispersion relation

For given a fixed energy, we have 4-state with different k_x .

$$\psi(E) = e^{ik_x x} \cdot \left[A \cdot e^{i\tilde{k}_y y} \cdot x_2 + B \cdot e^{ik_y y} \cdot x_1 + C \cdot e^{-ik_y y} \cdot \tilde{x}_1 + D \cdot e^{-i\tilde{k}_y y} \cdot \tilde{x}_2 \right] \cdot e^{-iEt} \quad (4.28)$$

Numerical Solve Eigen Energy.

$$\begin{aligned}
 A \cdot \tilde{r}_{11} + B \cdot \tilde{r}_{21} &= D \\
 A \cdot \tilde{r}_{12} + B \cdot \tilde{r}_{22} &= C \\
 C \cdot r_{21} + D \cdot r_{11} &= A \\
 C \cdot r_{22} + D \cdot r_{12} &= B
 \end{aligned}
 \Rightarrow
 \begin{bmatrix}
 \tilde{r}_{11} & \tilde{r}_{21} & 0 & -1 \\
 \tilde{r}_{12} & \tilde{r}_{22} & -1 & 0 \\
 -1 & 0 & r_{21} & r_{11} \\
 0 & -1 & r_{22} & r_{12}
 \end{bmatrix}
 \cdot
 \begin{bmatrix}
 A \\
 B \\
 C \\
 D
 \end{bmatrix}
 = 0
 \Rightarrow
 M \cdot
 \begin{bmatrix}
 A \\
 B \\
 C \\
 D
 \end{bmatrix}
 = 0
 \tag{4.29}$$

$$\begin{aligned}
 \det(M) &= -1 + (r_{12} \cdot \tilde{r}_{21} + r_{22} \cdot \tilde{r}_{22} + r_{21} \cdot \tilde{r}_{12} + r_{11} \cdot \tilde{r}_{11}) \\
 &\quad - (r_{12} \cdot r_{21} \cdot \tilde{r}_{12} \cdot \tilde{r}_{21} - r_{12} \cdot r_{21} \cdot \tilde{r}_{11} \cdot \tilde{r}_{22}) \\
 &\quad + (+r_{11} \cdot r_{22} \cdot \tilde{r}_{12} \cdot \tilde{r}_{21} - r_{11} \cdot r_{22} \cdot \tilde{r}_{11} \cdot \tilde{r}_{22})
 \end{aligned}
 \tag{4.30}$$

Eigen state

$$\begin{bmatrix}
 1 & 0 & -r_{21} & -r_{11} \\
 0 & 1 & -r_{22} & -r_{12} \\
 0 & 0 & 1 - r_{12} \cdot \tilde{r}_{12} - r_{22} \cdot \tilde{r}_{22} & -r_{11} \cdot \tilde{r}_{12} - r_{12} \cdot \tilde{r}_{22} \\
 0 & 0 & -r_{21} \cdot \tilde{r}_{11} - r_{22} \cdot \tilde{r}_{21} & 1 - r_{11} \cdot \tilde{r}_{11} - r_{12} \cdot \tilde{r}_{21}
 \end{bmatrix}
 \cdot
 \begin{bmatrix}
 A \\
 B \\
 C \\
 D
 \end{bmatrix}
 = 0
 \Rightarrow
 T \cdot
 \begin{bmatrix}
 A \\
 B \\
 C \\
 D
 \end{bmatrix}
 = 0
 \tag{4.31}$$

Therefore we can obtain Eigen state wave function by solving Eq. (4.31).

4.2 Matching boundary condition and scattering method

After having the eigen state in the quantum dot including subband mixing, we match boundary condition to solve this problem as the previous chapter.

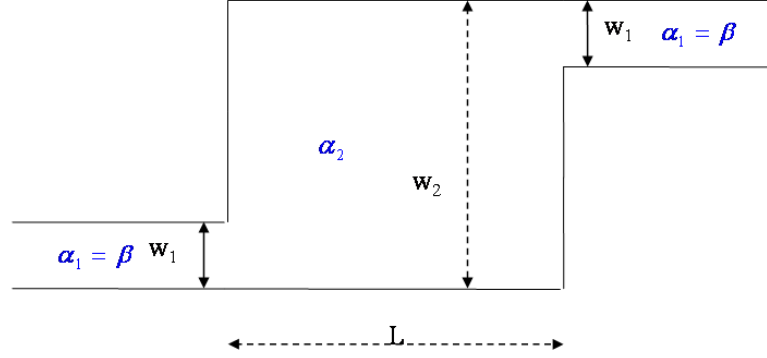


Figure 4.5: The model of open quantum dot.

$$\begin{aligned} \psi_{L1}(x, y) = & e^{ik_{n_0}x} \cdot e^{-i\frac{\alpha_1}{\sqrt{2}}x} \cdot \phi_{n_0}(y) \cdot \chi_+ \\ & + \sum_n \left[r_{n,+} \cdot e^{-i\frac{\alpha_1}{\sqrt{2}}x} \cdot \chi_+ + r_{n,-} \cdot e^{+i\frac{\alpha_1}{\sqrt{2}}x} \cdot \chi_- \right] \cdot e^{-ik_n x} \cdot \phi_n(y) \end{aligned} \quad (4.32)$$

In order to apply our formulation to evanesce mode, we rewrite the representation of spin state.

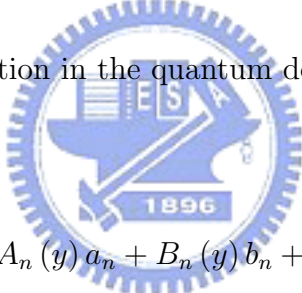
$$a_n = \frac{1}{\sqrt{1+f_1^2}} \cdot \begin{pmatrix} 1 \\ f_1 \end{pmatrix}, \quad f_1 = -i \frac{(k_{x,n} + i \cdot \tilde{k}_{y,n})}{\sqrt{k_{x,n}^2 + \tilde{k}_{y,n}^2}} \quad (4.33)$$

$$b_n = \frac{1}{\sqrt{1+f_2^2}} \cdot \begin{pmatrix} 1 \\ f_2 \end{pmatrix}, \quad f_2 = i \frac{(k_{x,n} + i \cdot k_{y,n})}{\sqrt{k_{x,n}^2 + k_{y,n}^2}} \quad (4.34)$$

$$c_n = \frac{1}{\sqrt{1+h_2^2}} \cdot \begin{pmatrix} 1 \\ h_2 \end{pmatrix}, \quad h_2 = i \frac{(k_{x,n} - i \cdot k_{y,n})}{\sqrt{k_{x,n}^2 + k_{y,n}^2}} \quad (4.35)$$

$$d_n = \frac{1}{\sqrt{1+h_1^2}} \cdot \begin{pmatrix} 1 \\ h_1 \end{pmatrix}, \quad h_1 = -i \frac{(k_{x,n} - i \cdot \tilde{k}_{y,n})}{\sqrt{k_{x,n}^2 + \tilde{k}_{y,n}^2}} \quad (4.36)$$

Write down the wave function in the quantum dot:



$$\begin{aligned} \psi_D &= \sum_n R_n \cdot e^{i\tilde{k}_n x} \cdot [A_n(y) a_n + B_n(y) b_n + C_n(y) c_n + D_n(y) d_n] \\ &+ \sum_n L_n \cdot e^{-i\tilde{k}_n x} \cdot [\tilde{A}_n(y) \tilde{a}_n + \tilde{B}_n(y) \tilde{b}_n + \tilde{C}_n(y) \tilde{c}_n + \tilde{D}_n(y) \tilde{d}_n] \end{aligned} \quad (4.37)$$

Write down the wave function in the lead:

$$\psi_{L2}(x, y) = \sum_n \left[t_{n,+} \cdot e^{-i\frac{\alpha_1}{\sqrt{2}}x} \cdot \chi_+ + t_{n,-} \cdot e^{+i\frac{\alpha_1}{\sqrt{2}}x} \cdot \chi_- \right] \cdot e^{ik_n x} \cdot \phi_n(y) \quad (4.38)$$

Match wave function continuous at $x = 0$:

$$\begin{aligned}
& \phi_{n_0}(y) \cdot \chi_+ + \sum_n [r_{n,+} \cdot \chi_+ + r_{n,-} \cdot \chi_-] \cdot \phi_n(y) \\
= & \sum_n \{R_n \cdot [A_n(y) a_n + B_n(y) b_n + C_n(y) c_n + D_n(y) d_n]\} \\
& + \sum_n \left\{ L_n \cdot [\tilde{A}_n(y) \tilde{a}_n + \tilde{B}_n(y) \tilde{b}_n + \tilde{C}_n(y) \tilde{c}_n + \tilde{D}_n(y) \tilde{d}_n] \right\} \tag{4.39}
\end{aligned}$$

Match slope of wave function continuous at $x = 0$. Put step function in our Hamiltonian to keep our Hamiltonian be hermitian operator.

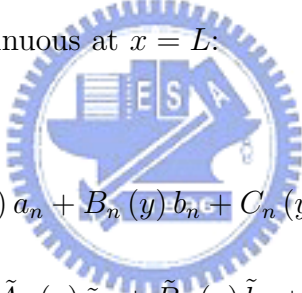
$$\left(\frac{\partial}{\partial x} + \frac{1}{2} i \cdot \alpha_2 \cdot \sigma_y \right) \cdot \psi|_{0+\varepsilon} = \left[\frac{\partial}{\partial x} + \frac{1}{2} i \cdot \alpha_1 \cdot (\sigma_x + \sigma_y) \right] \cdot \psi|_{0-\varepsilon} \tag{4.40}$$

$$\begin{aligned}
\sigma_y \cdot a_n &= \begin{bmatrix} 0 & -i \\ i & 0 \end{bmatrix} \cdot \frac{1}{\sqrt{2}} \begin{pmatrix} 1 \\ i \cdot e^{i\theta} \end{pmatrix} = \frac{1}{\sqrt{2}} e^{i\theta} \begin{pmatrix} 1 \\ i \cdot e^{-i\theta} \end{pmatrix} = e^{i\theta} \cdot d_n \\
\sigma_y \cdot b_n &= \begin{bmatrix} 0 & -i \\ i & 0 \end{bmatrix} \cdot \frac{1}{\sqrt{2}} \begin{pmatrix} 1 \\ -i \cdot e^{i\theta'} \end{pmatrix} = \frac{(-1)}{\sqrt{2}} e^{i\theta'} \begin{pmatrix} 1 \\ -i \cdot e^{-i\theta'} \end{pmatrix} = -e^{i\theta'} \cdot c_n \\
\sigma_y \cdot c_n &= \begin{bmatrix} 0 & -i \\ i & 0 \end{bmatrix} \cdot \frac{1}{\sqrt{2}} \begin{pmatrix} 1 \\ -i \cdot e^{-i\theta'} \end{pmatrix} = \frac{(-1)}{\sqrt{2}} e^{-i\theta'} \begin{pmatrix} 1 \\ -i \cdot e^{i\theta'} \end{pmatrix} = -e^{-i\theta'} \cdot b_n \\
\sigma_y \cdot d_n &= \begin{bmatrix} 0 & -i \\ i & 0 \end{bmatrix} \cdot \frac{1}{\sqrt{2}} \begin{pmatrix} 1 \\ i \cdot e^{-i\theta} \end{pmatrix} = \frac{1}{\sqrt{2}} e^{-i\theta} \begin{pmatrix} 1 \\ i \cdot e^{i\theta} \end{pmatrix} = e^{-i\theta} \cdot a_n
\end{aligned} \tag{4.41}$$

Put substitution Eq. (4.41) into Eq. (4.32) and Eq. (4.37).

$$\begin{aligned}
& k_{n_0} \cdot \phi_{n_0}(y) \cdot \chi_+ - \sum_n k_n \cdot [r_{n,+} \cdot \chi_+ + r_{n,-} \cdot \chi_-] \cdot \phi_n(y) \\
&= \sum_n R_n \cdot \tilde{k}_n \cdot [A_n(y) a_n + B_n(y) b_n + C_n(y) c_n + D_n(y) d_n] \\
&\quad - \frac{\alpha_2}{2} \cdot \sum_n R_n \cdot [A_n(y) \cdot e^{i\theta} \cdot d_n - B_n(y) \cdot e^{i\theta'} \cdot c_n - C_n(y) \cdot e^{-i\theta'} \cdot b_n + D_n(y) \cdot e^{-i\theta} \cdot a_n] \\
&\quad - \sum_n L_n \cdot \tilde{k}_n \cdot [\tilde{A}_n(y) \tilde{a}_n + \tilde{B}_n(y) \tilde{b}_n + \tilde{C}_n(y) \tilde{c}_n + \tilde{D}_n(y) \tilde{d}_n] \\
&\quad - \frac{\alpha_2}{2} \cdot \sum_n L_n \cdot [\tilde{A}_n(y) \cdot e^{i\theta} \cdot \tilde{d}_n - \tilde{B}_n(y) \cdot e^{i\theta'} \cdot \tilde{c}_n - \tilde{C}_n(y) \cdot e^{-i\theta'} \cdot \tilde{b}_n + \tilde{D}_n(y) \cdot e^{-i\theta} \cdot \tilde{a}_n]
\end{aligned} \tag{4.42}$$

Match wave function continuous at $x = L$:



$$\begin{aligned}
& \sum_n \left(R_n \cdot e^{i\tilde{k}_n L} \right) \cdot [A_n(y) a_n + B_n(y) b_n + C_n(y) c_n + D_n(y) d_n] \\
& \quad + \sum_n \left(L_n \cdot e^{-i\tilde{k}_n L} \right) \cdot [\tilde{A}_n(y) \tilde{a}_n + \tilde{B}_n(y) \tilde{b}_n + \tilde{C}_n(y) \tilde{c}_n + \tilde{D}_n(y) \tilde{d}_n] \\
&= \sum_n \left[t_{n,+} \cdot e^{ik_n L} \cdot e^{-i\frac{\alpha_1}{\sqrt{2}} L} \cdot \chi_+ + t_{n,-} \cdot e^{ik_n L} \cdot e^{+i\frac{\alpha_1}{\sqrt{2}} L} \cdot \chi_- \right] \cdot \phi_n(y)
\end{aligned} \tag{4.43}$$

Match slope of wave function continuous at $x = L$.

$$\begin{aligned}
& \sum_n R_n \cdot e^{i\tilde{k}_n L} \cdot \tilde{k}_n \cdot [A_n(y) a_n + B_n(y) b_n + C_n(y) c_n + D_n(y) d_n] \\
&\quad - \frac{\alpha_2}{2} \cdot \sum_n R_n \cdot e^{i\tilde{k}_n L} \cdot [A_n(y) \cdot e^{i\theta} \cdot d_n - B_n(y) \cdot e^{i\theta'} \cdot c_n - C_n(y) \cdot e^{-i\theta'} \cdot b_n + D_n(y) \cdot e^{-i\theta} \cdot a_n] \\
&\quad - \sum_n L_n \cdot e^{-i\tilde{k}_n L} \cdot \tilde{k}_n \cdot [\tilde{A}_n(y) \tilde{a}_n + \tilde{B}_n(y) \tilde{b}_n + \tilde{C}_n(y) \tilde{c}_n + \tilde{D}_n(y) \tilde{d}_n] \\
&\quad - \frac{\alpha_2}{2} \cdot \sum_n L_n \cdot e^{-i\tilde{k}_n L} \cdot [\tilde{A}_n(y) \cdot e^{i\theta} \cdot \tilde{d}_n - \tilde{B}_n(y) \cdot e^{i\theta'} \cdot \tilde{c}_n - \tilde{C}_n(y) \cdot e^{-i\theta'} \cdot \tilde{b}_n + \tilde{D}_n(y) \cdot e^{-i\theta} \cdot \tilde{a}_n] \\
&= \sum_n k_n \cdot \left[t_{n,+} \cdot e^{ik_n L} \cdot e^{-i\frac{\alpha_1}{\sqrt{2}} L} \cdot \chi_+ + t_{n,-} \cdot e^{ik_n L} \cdot e^{+i\frac{\alpha_1}{\sqrt{2}} L} \cdot \chi_- \right] \cdot \phi_n(y)
\end{aligned}$$

(4.44)

Multiplying Eq. (4.39) by $\int_0^{w_1} [A_n(y) a_n + B_n(y) b_n + C_n(y) c_n + D_n(y) d_n]^+ dy$, we obtain:

$$\begin{aligned}
 & [A_{m,n_0}^L \cdot a_m^+ \cdot \chi_+ + B_{m,n_0}^L \cdot b_m^+ \cdot \chi_+ + C_{m,n_0}^L \cdot c_m^+ \cdot \chi_+ + D_{m,n_0}^L \cdot d_m^+ \cdot \chi_+] \\
 & + \sum_n [(A_{m,n}^L \cdot a_m^+ \cdot \chi_+ + B_{m,n}^L \cdot b_m^+ \cdot \chi_+ + C_{m,n}^L \cdot c_m^+ \cdot \chi_+ + D_{m,n}^L \cdot d_m^+ \cdot \chi_+) \cdot r_{n,+}] \\
 & + \sum_n [(A_{m,n}^L \cdot a_m^+ \cdot \chi_- + B_{m,n}^L \cdot b_m^+ \cdot \chi_- + C_{m,n}^L \cdot c_m^+ \cdot \chi_- + D_{m,n}^L \cdot d_m^+ \cdot \chi_-) \cdot r_{n,-}] \\
 & = \sum_n (R_n \cdot \delta_{m,n} + L_n \cdot G_{m,n})
 \end{aligned} \tag{4.45}$$

where the matrix element is defined by following representation:

$$A_{m,n}^L = A_m^* \cdot \int_0^d e^{-i\tilde{k}_y y} \cdot \phi_n(y) \cdot dy, \quad \tilde{A}_{m,n}^L = \tilde{A}_m^* \cdot \int_0^d e^{-i\tilde{k}_y y} \cdot \phi_n(y) \cdot dy \tag{4.46}$$

$$B_{m,n}^L = B_m^* \cdot \int_0^d e^{-ik_y y} \cdot \phi_n(y) \cdot dy, \quad \tilde{B}_{m,n}^L = \tilde{B}_m^* \cdot \int_0^d e^{-ik_y y} \cdot \phi_n(y) \cdot dy \tag{4.47}$$

$$C_{m,n}^L = C_m^* \cdot \int_0^d e^{ik_y y} \cdot \phi_n(y) \cdot dy, \quad \tilde{C}_{m,n}^L = \tilde{C}_m^* \cdot \int_0^d e^{ik_y y} \cdot \phi_n(y) \cdot dy \tag{4.48}$$

$$D_{m,n}^L = D_m^* \cdot \int_0^d e^{i\tilde{k}_y y} \cdot \phi_n(y) \cdot dy, \quad \tilde{D}_{m,n}^L = \tilde{D}_m^* \cdot \int_0^d e^{i\tilde{k}_y y} \cdot \phi_n(y) \cdot dy \tag{4.49}$$

and

$$\begin{aligned}
 G_{m,n} & = \int_0^{w_2} [A_n(y) a_n + B_n(y) b_n + C_n(y) c_n + D_n(y) d_n]^+ \cdot \\
 & \quad [\tilde{A}_n(y) \tilde{a}_n + \tilde{B}_n(y) \tilde{b}_n + \tilde{C}_n(y) \tilde{c}_n + \tilde{D}_n(y) \tilde{d}_n] dy
 \end{aligned} \tag{4.50}$$

Multiplying Eq. (4.42) by $\chi_{\pm}^* \cdot \int_0^{w_1} \phi_{n'}(y) dy$, we obtain

$$\begin{aligned}
& k_{n_0} - \sum_n r_{n,+} \cdot k_n \cdot \delta_{m,n} \\
&= \sum_n R_n \cdot \tilde{k}_n \cdot \left[(A_{m,n}^L)^+ \cdot \chi_+^+ \cdot a_n + (B_{m,n}^L)^+ \cdot \chi_+^+ \cdot b_n + (C_{m,n}^L)^+ \cdot \chi_+^+ \cdot c_n + (D_{m,n}^L)^+ \cdot \chi_+^+ \cdot d_n \right] \\
&- \frac{\alpha_2}{2} \cdot \sum_n R_n \cdot \left[\begin{array}{l} (A_{m,n}^L)^+ \cdot e^{i\theta} \cdot \chi_+^+ \cdot d_n - (B_{m,n}^L)^+ \cdot e^{i\theta'} \cdot \chi_+^+ \cdot c_n \\ - (C_{m,n}^L)^+ \cdot e^{-i\theta'} \cdot \chi_+^+ \cdot b_n + (D_{m,n}^L)^+ \cdot e^{-i\theta} \cdot \chi_+^+ \cdot a_n \end{array} \right] \\
&- \sum_n L_n \cdot \tilde{k}_n \cdot \left[(\tilde{A}_{m,n}^L)^+ \cdot \chi_+^+ \cdot a_n + (\tilde{B}_{m,n}^L)^+ \cdot \chi_+^+ \cdot b_n + (\tilde{C}_{m,n}^L)^+ \cdot \chi_+^+ \cdot c_n + (\tilde{D}_{m,n}^L)^+ \cdot \chi_+^+ \cdot d_n \right] \\
&- \frac{\alpha_2}{2} \cdot \sum_n L_n \cdot \left[\begin{array}{l} (\tilde{A}_{m,n}^L)^+ \cdot e^{i\theta} \cdot \chi_+^+ \cdot d_n - (\tilde{B}_{m,n}^L)^+ \cdot e^{i\theta'} \cdot \chi_+^+ \cdot c_n \\ - (\tilde{C}_{m,n}^L)^+ \cdot e^{-i\theta'} \cdot \chi_+^+ \cdot b_n + (\tilde{D}_{m,n}^L)^+ \cdot e^{-i\theta} \cdot \chi_+^+ \cdot a_n \end{array} \right]
\end{aligned} \tag{4.51}$$

and



$$\begin{aligned}
& - \sum_n r_{n,-} \cdot k_n \cdot \delta_{m,n} \\
&= \sum_n R_n \cdot \tilde{k}_n \cdot \left[(A_{m,n}^L)^+ \cdot \chi_-^+ \cdot a_n + (B_{m,n}^L)^+ \cdot \chi_-^+ \cdot b_n + (C_{m,n}^L)^+ \cdot \chi_-^+ \cdot c_n + (D_{m,n}^L)^+ \cdot \chi_-^+ \cdot d_n \right] \\
&- \frac{\alpha_2}{2} \cdot \sum_n R_n \cdot \left[\begin{array}{l} (A_{m,n}^L)^+ \cdot e^{i\theta} \cdot \chi_-^+ \cdot d_n - (B_{m,n}^L)^+ \cdot e^{i\theta'} \cdot \chi_-^+ \cdot c_n \\ - (C_{m,n}^L)^+ \cdot e^{-i\theta'} \cdot \chi_-^+ \cdot b_n + (D_{m,n}^L)^+ \cdot e^{-i\theta} \cdot \chi_-^+ \cdot a_n \end{array} \right] \\
&- \sum_n L_n \cdot \tilde{k}_n \cdot \left[(\tilde{A}_{m,n}^L)^+ \cdot \chi_-^+ \cdot a_n + (\tilde{B}_{m,n}^L)^+ \cdot \chi_-^+ \cdot b_n + (\tilde{C}_{m,n}^L)^+ \cdot \chi_-^+ \cdot c_n + (\tilde{D}_{m,n}^L)^+ \cdot \chi_-^+ \cdot d_n \right] \\
&- \frac{\alpha_2}{2} \cdot \sum_n L_n \cdot \left[\begin{array}{l} (\tilde{A}_{m,n}^L)^+ \cdot e^{i\theta} \cdot \chi_-^+ \cdot d_n - (\tilde{B}_{m,n}^L)^+ \cdot e^{i\theta'} \cdot \chi_-^+ \cdot c_n \\ - (\tilde{C}_{m,n}^L)^+ \cdot e^{-i\theta'} \cdot \chi_-^+ \cdot b_n + (\tilde{D}_{m,n}^L)^+ \cdot e^{-i\theta} \cdot \chi_-^+ \cdot a_n \end{array} \right]
\end{aligned} \tag{4.52}$$

Define matrix element by following representation:

$$A_{m,n}^R = A_m^* \cdot \int_0^d e^{-i\tilde{k}_y y} \cdot \phi_n(y) \cdot dy, \quad \tilde{A}_{m,n}^R = \tilde{A}_m^* \cdot \int_0^d e^{-i\tilde{k}_y y} \cdot \phi_n(y) \cdot dy \quad (4.53)$$

$$B_{m,n}^R = B_m^* \cdot \int_0^d e^{-ik_y y} \cdot \phi_n(y) \cdot dy, \quad \tilde{B}_{m,n}^R = \tilde{B}_m^* \cdot \int_0^d e^{-ik_y y} \cdot \phi_n(y) \cdot dy \quad (4.54)$$

$$C_{m,n}^R = C_m^* \cdot \int_0^d e^{ik_y y} \cdot \phi_n(y) \cdot dy, \quad \tilde{C}_{m,n}^R = \tilde{C}_m^* \cdot \int_0^d e^{ik_y y} \cdot \phi_n(y) \cdot dy \quad (4.55)$$

$$D_{m,n}^R = D_m^* \cdot \int_0^d e^{i\tilde{k}_y y} \cdot \phi_n(y) \cdot dy, \quad \tilde{D}_{m,n}^R = \tilde{D}_m^* \cdot \int_0^d e^{i\tilde{k}_y y} \cdot \phi_n(y) \cdot dy \quad (4.56)$$

Multiplying Eq. (4.43) by $\int_0^{w_1} [A_n(y) a_n + B_n(y) b_n + C_n(y) c_n + D_n(y) d_n]^+ dy$, we obtain:

$$\begin{aligned} & \sum_n \left[R_n \cdot e^{i\tilde{k}_n L} \cdot \delta_{m,n} + L_n \cdot e^{-i\tilde{k}_n L} \cdot G_{m,n} \right] \\ &= \sum_n \left[t_{n,+} \cdot e^{ik_n L} \cdot e^{-i\frac{\alpha_1}{\sqrt{2}} L} \cdot (A_{m,n}^R \cdot a_m^* \cdot \chi_+ + B_{m,n}^R \cdot b_m^* \cdot \chi_+ + C_{m,n}^R \cdot c_m^* \cdot \chi_+ + D_{m,n}^R \cdot d_m^* \cdot \chi_+) \right] \\ &+ \sum_n \left[+t_{n,-} \cdot e^{ik_n L} \cdot e^{+i\frac{\alpha_1}{\sqrt{2}} L} \cdot (A_{m,n}^R \cdot a_m^* \cdot \chi_- + B_{m,n}^R \cdot b_m^* \cdot \chi_- + C_{m,n}^R \cdot c_m^* \cdot \chi_- + D_{m,n}^R \cdot d_m^* \cdot \chi_-) \right] \end{aligned} \quad (4.57)$$

Multiplying Eq. (4.44) by $\chi_{\pm}^* \cdot \int_0^{w_1} \phi_{n'}(y) dy$, we obtain

$$\begin{aligned}
 & \sum_n R_n \cdot e^{i\tilde{k}_n L} \cdot \tilde{k}_n \cdot \left[(A_{m,n}^R)^+ \cdot \chi_+^+ \cdot a_n + (B_{m,n}^R)^+ \cdot \chi_+^+ \cdot b_n + (C_{m,n}^R)^+ \cdot \chi_+^+ \cdot c_n + (D_{m,n}^R)^+ \cdot \chi_+^+ \cdot d_n \right] \\
 & - \frac{\alpha_2}{2} \cdot \sum_n R_n \cdot e^{i\tilde{k}_n L} \cdot \left[(A_{m,n}^R)^+ \cdot e^{i\theta} \cdot \chi_+^+ \cdot d_n - (B_{m,n}^R)^+ \cdot e^{i\theta'} \cdot \chi_+^+ \cdot c_n \right. \\
 & \quad \left. - (C_{m,n}^R)^+ \cdot e^{-i\theta'} \cdot \chi_+^+ \cdot b_n + (D_{m,n}^R)^+ \cdot e^{-i\theta} \cdot \chi_+^+ \cdot a_n \right] \\
 & - \sum_n L_n \cdot e^{-i\tilde{k}_n L} \cdot \tilde{k}_n \cdot \left[(\tilde{A}_{m,n}^R)^+ \cdot \chi_+^+ \cdot a_n + (\tilde{B}_{m,n}^R)^+ \cdot \chi_+^* \cdot b_n \right. \\
 & \quad \left. + (\tilde{C}_{m,n}^R)^+ \cdot \chi_+^+ \cdot c_n + (\tilde{D}_{m,n}^R)^+ \cdot \chi_+^+ \cdot d_n \right] \\
 & - \frac{\alpha_2}{2} \cdot \sum_n L_n \cdot e^{-i\tilde{k}_n L} \cdot \left[(\tilde{A}_{m,n}^R)^+ \cdot e^{i\theta} \cdot \chi_+^+ \cdot d_n - (\tilde{B}_{m,n}^R)^+ \cdot e^{i\theta'} \cdot \chi_+^+ \cdot c_n \right. \\
 & \quad \left. - (\tilde{C}_{m,n}^R)^+ \cdot e^{-i\theta'} \cdot \chi_+^+ \cdot b_n + (\tilde{D}_{m,n}^R)^+ \cdot e^{-i\theta} \cdot \chi_+^+ \cdot a_n \right] \\
 & = \sum_n \left[t_{n,+} \cdot e^{ik_n L} \cdot e^{-i\frac{\alpha_1}{\sqrt{2}}L} \cdot k_n \cdot \delta_{m,n} \right]
 \end{aligned} \tag{4.58}$$

and

$$\begin{aligned}
 & \sum_n R_n \cdot e^{i\tilde{k}_n L} \cdot \tilde{k}_n \cdot \left[(A_{m,n}^R)^+ \cdot \chi_-^+ \cdot a_n + (B_{m,n}^R)^+ \cdot \chi_-^+ \cdot b_n + (C_{m,n}^R)^+ \cdot \chi_-^+ \cdot c_n + (D_{m,n}^R)^+ \cdot \chi_-^+ \cdot d_n \right] \\
 & - \frac{\alpha_2}{2} \cdot \sum_n R_n \cdot e^{i\tilde{k}_n L} \cdot \left[(A_{m,n}^R)^+ \cdot e^{i\theta} \cdot \chi_-^+ \cdot d_n - (B_{m,n}^R)^+ \cdot e^{i\theta'} \cdot \chi_-^+ \cdot c_n \right. \\
 & \quad \left. - (C_{m,n}^R)^+ \cdot e^{-i\theta'} \cdot \chi_-^+ \cdot b_n + (D_{m,n}^R)^+ \cdot e^{-i\theta} \cdot \chi_-^+ \cdot a_n \right] \\
 & - \sum_n L_n \cdot e^{-i\tilde{k}_n L} \cdot \tilde{k}_n \cdot \left[(A_{m,n}^R)^+ \cdot \chi_-^+ \cdot a_n + (B_{m,n}^R)^+ \cdot \chi_-^+ \cdot b_n \right. \\
 & \quad \left. + (C_{m,n}^R)^+ \cdot \chi_-^+ \cdot c_n + (D_{m,n}^R)^+ \cdot \chi_-^+ \cdot d_n \right] \\
 & - \frac{\alpha_2}{2} \cdot \sum_n L_n \cdot e^{-i\tilde{k}_n L} \cdot \left[(\tilde{A}_{m,n}^R)^+ \cdot e^{i\theta} \cdot \chi_-^+ \cdot d_n - (\tilde{B}_{m,n}^R)^+ \cdot e^{i\theta'} \cdot \chi_-^+ \cdot c_n \right. \\
 & \quad \left. - (\tilde{C}_{m,n}^R)^+ \cdot e^{-i\theta'} \cdot \chi_-^+ \cdot b_n + (\tilde{D}_{m,n}^R)^+ \cdot e^{-i\theta} \cdot \chi_-^+ \cdot a_n \right] \\
 & = \sum_n \left[t_{n,-} \cdot e^{ik_n L} \cdot e^{+i\frac{\alpha_1}{\sqrt{2}}L} \cdot k_n \cdot \delta_{m,n} \right]
 \end{aligned} \tag{4.59}$$

Combine Eq. (4.45), Eq. (4.51), Eq. (4.57) and Eq. (4.58), we can use scattering

CHAPTER 4. QUANTUM TRANSPORT THROUGH A RASHBA-TYPE SPIN-ORBIT OPEN QUANTUM DOT: INCLUDING SUBBAND MIXING

method as the previous section to obtain the transmission rate and reflection rate.



Chapter 5

Spin-dependent current and numerical result

In this chapter, we show the numerical results and discussions of Quantum transport through a Rashba-type spin-orbit open quantum dot including subband mixing.

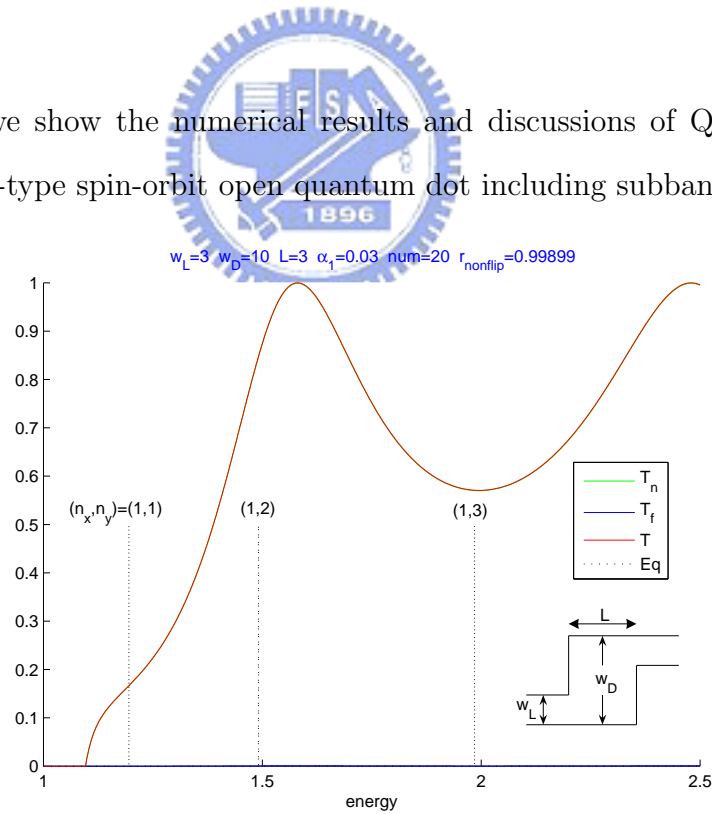


Figure 5.1: Open quantum dot with spin-orbit interaction in the absence of subband mixing under asymmetric structure

Before discuss the numerical result of chapter 4, we review chapter 3 at first. Fig. 5.1 is the numerical result by neglecting subband mixing. The structure is asymmetric as sketch in Fig. 5.1. w_D is the width of the open quantum dot and L is the its length. w_L is the width of lead. Assume the spin direction in the lead is determined.

T is total transmission, T_n is the transmission which spin direction doesn't flip and T_f is which spin direction flip. E_q is the energy of bound state in closed dot. α_L is the strength of Rashba effect in the lead and α_D is that in th open quantum dot. The number of subband is 20 in our calculation.

According the conclusion of chapter 3, We know the ratio of spin flipping is only depend on α_D . We give small $\alpha_D = 0.03$ in Fig. 5.1, so the ratio of spin non-flipping $r_{nonflip}$ is 0.99899 so closed to 1. Therefore T_n is very closed to T and T_f approaches to zero.

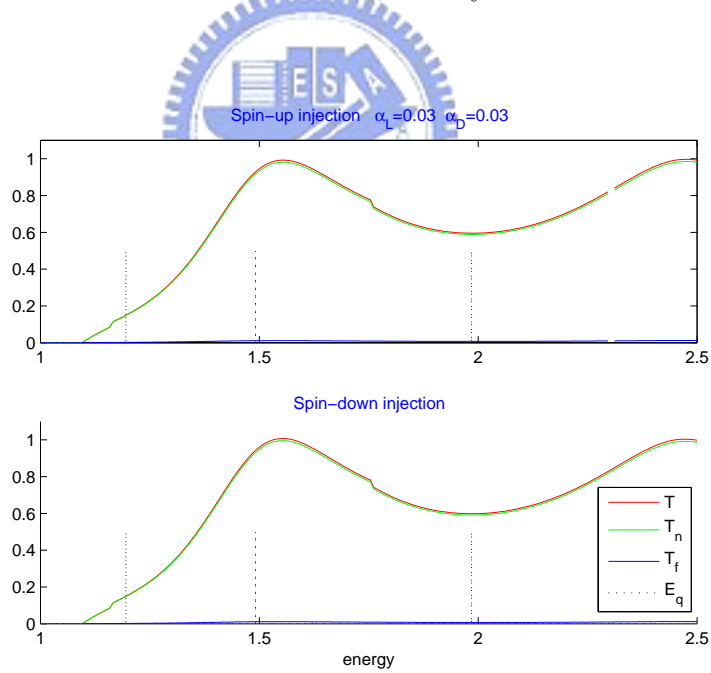


Figure 5.2: Open quantum dot including spin-orbit interaction and subband mixing under asymmetric structure

Fig. 5.2 is the same structure as Fig. 5.1. But we notice that Fig. 5.2 is not obviously different from Fig. 5.1. Although we can calculate the ratio of spin flipping numerically, but it is still too small to observe.

Surprisingly, transmission is depend on the direction of spin-injection. But the difference of transmission is very small to give us confidence to make conclusion.

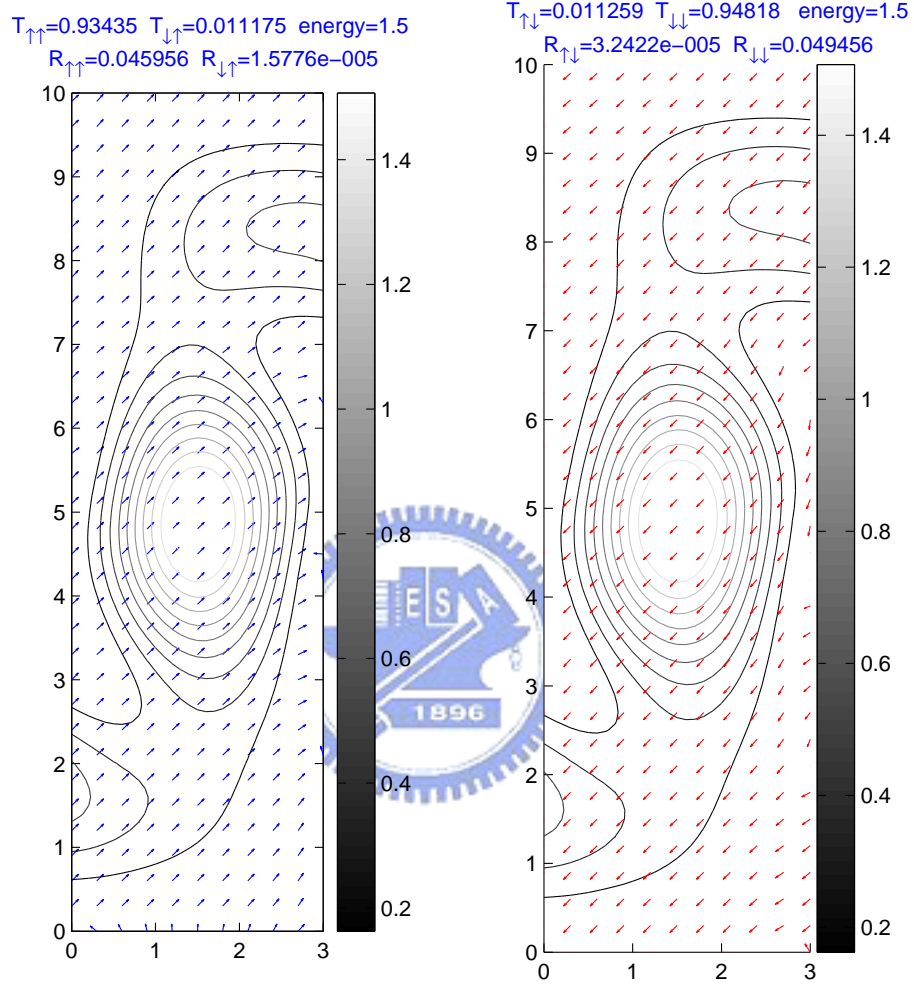


Figure 5.3: Spin precession distribution and the number of density in the open quantum dot

Fig. 5.3 is the spin precession distribution and the number of density in the quantum dot with the structure of Fig. 5.2. The incident energy is 1.5 with the unit $E^* = \frac{\hbar^2 \pi^2 k_F^2}{2m^*}$. $T_{\downarrow\uparrow}$ means the spin-down transmission coefficient under spin-up injection. $R_{\downarrow\uparrow}$ means the spin-down reflection coefficient under spin-up injection. We observe strong spin precession on the boundary of open quantum dot. Obviously, the reflection coefficient $R_{\downarrow\uparrow}$ and $R_{\uparrow\downarrow}$ is closed to zero.

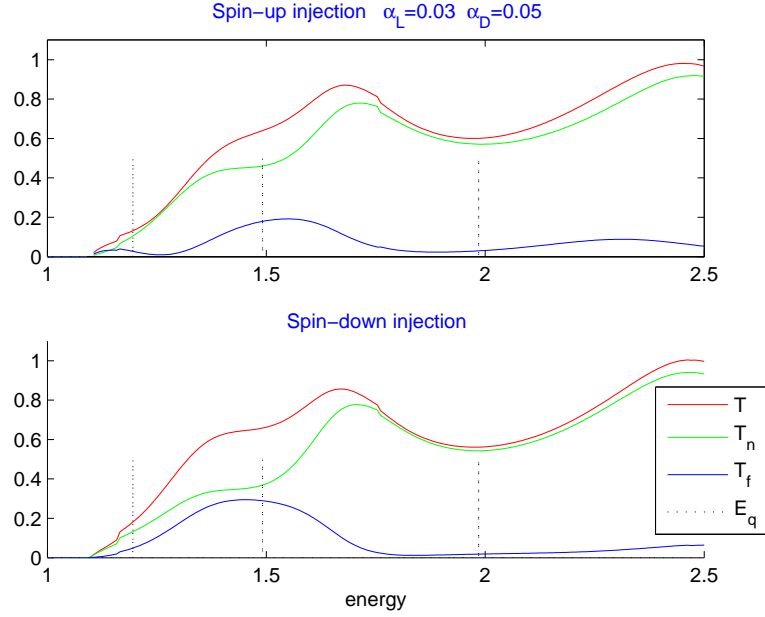


Figure 5.4: Open quantum dot including spin-orbit interaction with $\alpha_D=0.05$ which is stronger than Fig. 5.2

In Fig. 5.4, we tune the strength of Rashba effect in the open quantum dot α_D up to 0.05 with the unit $\frac{\hbar}{2m}$. Surprisingly, although we didn't tune the Rashba effect very much, we observe obvious transmission depend on spin injection near the quasi-bound state $(n_x, n_y) = (1, 2)$. But this feature is indistinct in $(n_x, n_y) = (1, 3)$. Through calculation, we obtain the ratio of spin non-flipping in the absence of subband mixing under this condition is 0.99719. So the spin-coupling due to subband mixing is very strong in this case.

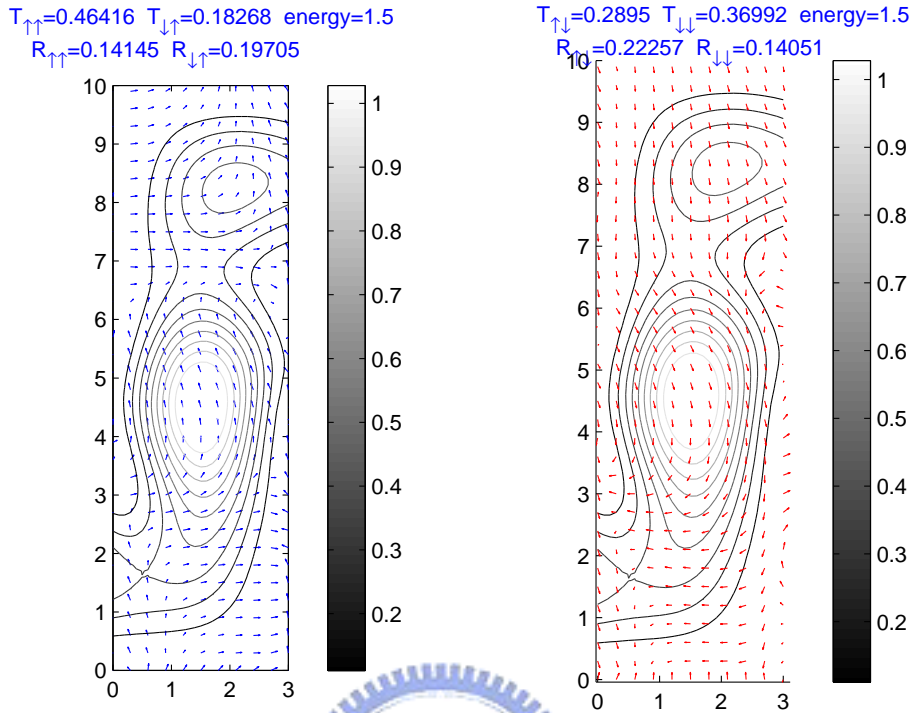


Figure 5.5: Spin precession distribution and the number of density in the open quantum dot with $\alpha_D=0.05$

We can see obvious spin precession in the open quantum dot in Fig. 5.5. Not only in boundary of the quantum dot, but also the center of the open quantum dot can see clear spin precession. Notice that, the boundary of lead and open quantum dot can see strong spin precession effect than Fig. 5.2.

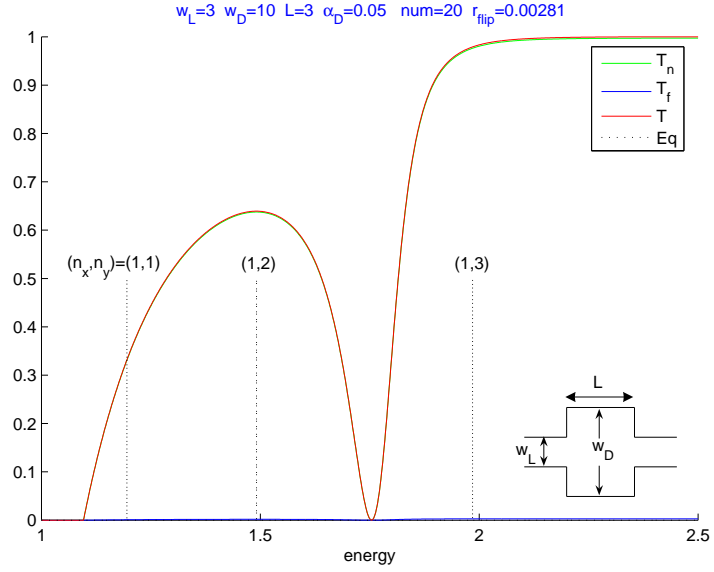


Figure 5.6: Open quantum dot with spin-orbit interaction in the absence of subband mixing under symmetric structure

In order to get more clear resonance structure, we design a symmetric structure to neglect wave function coupling of odd and even. So resonance near quasi bound state $(n_x, n_y) = (1, 2)$ will disappear. Only resonance near quasi bound state $(n_x, n_y) = (1, 3)$ can be observed in Fig. 5.6. This resonance dip can approach to zero very closely.

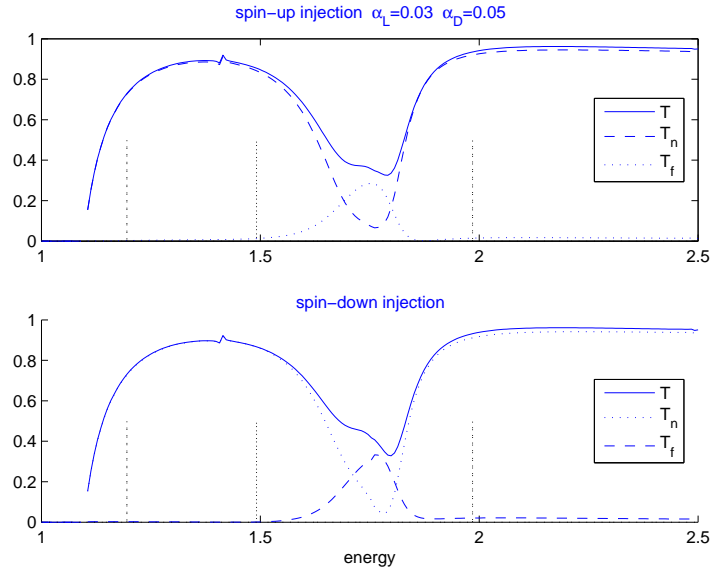


Figure 5.7: Open quantum dot including spin-orbit interaction and subband mixing under asymmetric structure

In Fig. 5.7, we see the strong spin flipping on the resonance dip. And the resonance dip didn't approach to zero due to strong spin flipping. Interestingly, the electron with spin flipping can pass through the open quantum dot on resonance dip. Compare the figure of spin-up injection and spin-down injection, we also can observe spin-dependent transmission.

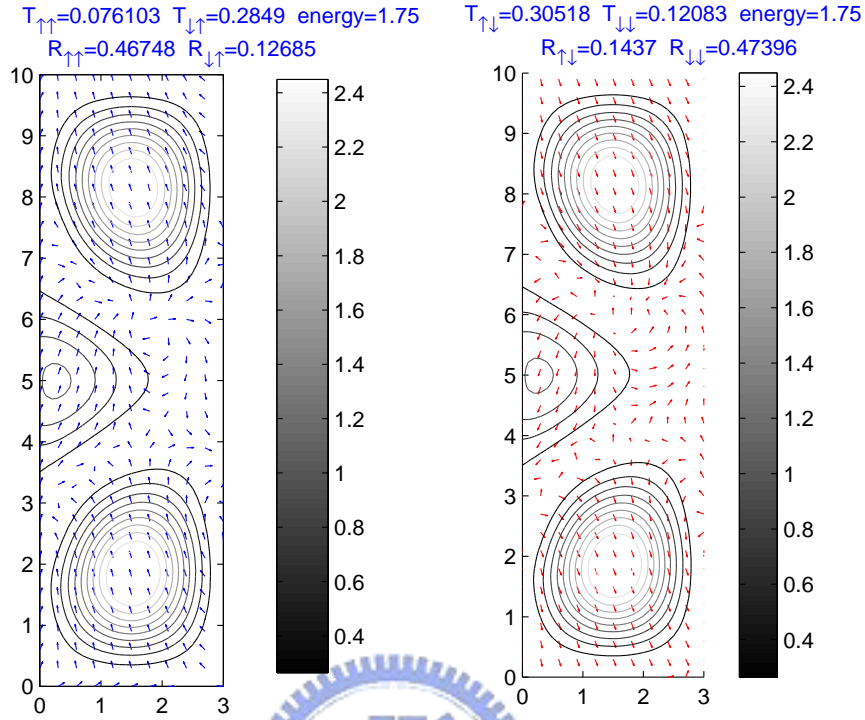


Figure 5.8: Spin precession distribution and the number of density in the open quantum dot with $\alpha_D=0.05$ under symmetric structure

Fig. 5.8 is very different from Fig. 5.3 and Fig. 5.5. And we can see the spin rotate almost 180° from left lead to right. It can explain why the transmission of spin flipping is stronger than the transmission of spin non-flipping. This feature gives us confidence to our numerical result.

Chapter 6

Conclusion and Future work

In chapter 2, we use custom method to induce numerical de-phase process in 1 dimension case to solve 2 dimension problem through considering subband mixing. De-coherent strength $\varepsilon = 0$ occurs when double QPCs in series and coherent length is infinite. If de-coherent strength is raising up, the total conductance approaches the classical theoretical results and the de-coherent process increase the resistance so that total conductance is lowering down. But there is a special case. If resonance occurs, de-coherent strength cancel the effect of resonance but increase the resistance at the same time. If cancelation of resonance is more important, the resistance is increasing.

Through this conclusion, in future work, we may find out the relation of dwell time and coherent length.

In chapter 3, neglecting the subband mixing in calculation means we drop the possibility the spin precession at the same time. Transmission is independent of spin injection, and the ratio of spin flipping is independent of the shape of quantum dot, incident energy, and Rashba and Dresselhaus effect in the lead.

In chapter 5, we can see spin precession in the open quantum dot and transmission is depend on spin injection. These feature especially occurs on resonance structure. Another interesting point is that we can always suppress the spin precession by properly arranging the injected spin. In the next, we will try to control the direction of spin injection. We may

CHAPTER 6. CONCLUSION AND FUTURE WORK

want to know if geometry of quantum dot will influence the transmission, is it possible the current will turn another direction different from its original direction without applying magnetic field just depend on spin-orbit interaction?

Still lots of work we must to do.



Bibliography

- [1] S. Datta and B. Das, *Spply. Phys. Lett.* 56,665(1990)
- [2] E.I. Rashba, *Fiz. Tverd. Tela (Leningrad)* 2,1224(1960) [*Sov. Phys. Solid State* 2,1109(1960)]; Y.A. Bychkov and E.I. Rashba, *J. Phys. C* 17, 6039(1984).
- [3] G. Dresselhaus, *Phys. Rev.* 100,580 (1955)
- [4] M.I. Dyakonov and V.Y. Kachorovskii, *Sov. Phys. Semicond.* 20,110 (1986)
- [5] G. Bastard and R. Ferreira, *Surf. Sci.* 267, 335(1992)
- [6] R. Landauer, *IBM J. Res. Dev.* 1,223(1957)
- [7] R. Landauer, *Phil. Mag.* 21,863 (1970)
- [8] P.W. Anderson, D.J. Thouless, E. Abrahams, and D. S.Fisher, *Phys. Rev. B* 22,3519 (1980)
- [9] A.D. Stone and A. Szafer, *IBM J. Res. Dev.* 32,384(1988)
- [10] E.N. Economon and C.M. Soukoulis, Szafer, *Phys. Rev. Lett.* 46,618 (1981)
- [11] *Introduction to Mesoscopic Physics*, Y.Imry (Oxford 1997), pp94
- [12] M. Buttiker, Y.Imry, R.Landauer, and S.Pinhas, *Phys. Rev. B* 31,6207 (1985)
- [13] M. Buttiker, *Phys. Rev. Lett.* 57,1761 (1986)
- [14] A.D. Benoit, S. Washburn, C.P. Umbach, R. B. Laibowitz, and R.A. Webb, *Phys. Rev. Lett.* 57,1765 (1986)